Fall 11-13-2017

TENSILE EXPERIMENTATION OF STRUCTURAL ALUMINUM STUDYING VOID GROWTH

Scott Gampert

Scott Gampert

Candidate

Mechanical Engineering

Department

This thesis is approved, and it is acceptable in quality and form for publication:

Approved by the Thesis Committee:

Tariq Khraishi , Chairperson

Yu-Lin Shen

Mehran Tehrani

TENSILE EXPERIMENTATION OF STRUCTURAL ALUMINUM STUDYING VOID GROWTH

BY

SCOTT GAMPERT

BACHELOR OF SCIENCE
MECHANICAL ENGINEERING
UNIVERSITY OF NEW MEXICIO

THESIS

Submitted in Partial Fulfillment of the
Requirements for the Degree of

Master of Science
Mechanical Engineering

The University of New Mexico
Albuquerque, New Mexico

December 2017

ACKNOWLEDGEMENT

I would like to thank Professor Khraishi for mentoring me throughout my educational journey at the University of New Mexico. I would also like to thank the Earth and Planetary Sciences Department, in particular research Associate Professor Ying-Bing Jiang, for his help in calibrating and training me on the Scanning Electron Microscope (SEM).

The work on Atomic Force Microscope (AFM) was performed at the Center for Integrated Nanotechnologies, an Office of Science User Facility operated for the U.S. Department of Energy (DOE) Office of Science. Sandia National Laboratories is a multi-mission laboratory managed and operated by National Technology and Engineering Solutions of Sandia, LLC., a wholly owned subsidiary of Honeywell International, Inc., for the U.S. Department of Energy's National Nuclear Security Administration under contract DE-NA-0003525. A special thanks to Dr. Ezra Bussmann for taking his time to meet with me and personal involve himself in helping me to run the AFM analysis.

Additionally, I would to thank Dr. Shen and Dr. Tehrani, who took the time to be part of my thesis committee. Your added knowledge and experience helped me along the way.

TENSILE EXPERIMENTATION OF STRUCTURAL ALUMINUM STUDYING VOID GROWTH

By

Scott Gampert

Bachelor of Science, Mechanical Engineering. The University of New Mexico, 2014

Master of Science, Mechanical Engineering. The University of New Mexico, 2017

Abstract

Uni-axial tensile tests were conducted on multiple dog-bone shaped poly-crystalline Aluminum specimens. The goal for this study was to understand the effects of voiding in structural aluminum and how voids grow under tension. The voids were represented by simply drilling and reaming one or more holes in varying patterns in the center of the sample. The testing clearly showed that the different hole patterns affect the area growth of voids. It also compares the developmental growth of a plasticity zone around samples with one hole to a previous study done with a different specimen shape(Ray,2003). In order to look at the microscale of the plastic deformation, a Scanning Electric Microscope (SEM) was used to examine the samples. To look at the Nano scale of the plastic deformation, Atomic Force Microscopy (AFM) experiments were performed at multiple locations on various samples pulled to different levels of stress.

Contents

Table of Figures

Introduction

Overview

Studying void growth is an ever-growing field of interest especially in metallic materials such as aluminum 6061-T6. The reason behind this increasing interest is because a void can be considered the main cause of failures in everything that is built. These voids can be created from any number of steps in the process of creating the final parts. These voids can appear in the way the material is prepared. An example of this is how or if the material is heat treated.

Other reasons behind these failures might be how the material was machined or altered. These voids that are introduced into the material through the multiple steps of preparing the material will coalesce into larger voids causing parts to fail (Mulholland et al.,2006). Because these failures can range from being slightly annoying, like having pencil break on you, all the way to causing death from something like the part on a plane breaking during flight, it is extremely important to know how materials will fail.

A large majority of literature revolves around the theoretical and numerical aspects of how voids will react such as Irwin (1957), Dugdale (1960), Banks and Garlick (1984), Guerra-Rosa et al. (1984), Jing (2003, 2004), Unger (1990), Erdogan and Sih (1963), Theocaris and Andrianopolous (1982), Yehia (1991), Iida and Kobayashi (1969) and Golos and Wasiluk (2000), Dodds et al.(1991), Mishra and Parida (1985), Baxevanis et al. (2012), Theocaris et al. (1982), Kong et al. (1995), and Vallejo (1987). This is a good start into understanding how voids will behave but these papers only give us an estimation of how a failure might occur. These results can only be thought of as a “ball-

park" estimation, because reality does not always follow the perfect assumptions that are made so that these equations will work (Boyce et al.,2014).

Although a majority of the literature is based on theoretical studies, there are still multiple experimental studies. There have been many experimental studies that revolved around the use of superplastic materials. In 1979, Tait and Taplin studied superplastic materials under tension with a single predrilled hole. In 1982, Ghosh and Hamilton studied the strain sensitivity of the material when placed under tension. Next Khraishi et al. (2001) considered how superplastic behavior was affected with multiple holes while looking at its strain sensitivity and comparing it against a finite element analysis. Mulholland et al. (2006) studied how changing the strain rate with multiple holes can affect how far the superplastic specimens can be stretched.

Although aluminum does not have the same unique characteristics as the superplastic materials, the strength and light weight feature are very desirable when creating durable components. In 2003, Ray experimented with 6061-T6 using a cylinder that has a section removed to make a flat surface with one or two holes which was then polished and pulled in tension. Mae et al. (2008) studied how an aluminum component cast in sand compare to cast iron molds using round and butterfly shaped specimens. Tan et al. (2009) considered the hardness of artificially aged 6061-T6 aluminum by varying the amount of time at different temperatures used during the hardening process. Zhu et al. (2011) experimented using 6061-T6 aluminum with different strain rates to see how it would affect the fracture morphology. Zeng (2012) added extra magnesium to 6061-T6 aluminum and tested to check how this would affect the fatigue limit of the specimens. Shikama (2012) and Takahashi(2014) used a cylindrical sample of 6061-T6 with a small

artificial hole partially drilled into the center which they then tested to find what change would be created when reaching the fatigue limit. In most of these papers, they did not just consider the common fracture criteria, such as the stress strain curve, but also how the surface changes during the stretching process. The surface will begin to change based on how much tension it takes before the material necks. This is when the material is being pulled in one direction causing the material to slightly shrink in the other directions for the part to complete the stretch. During this period of stretching the material will create voids from imperfections in the material which coalesce into larger voids causing the specimens to ultimately break (Mullholland et al., 2006). It is very difficult, to almost impossible, to know where a void will appear in a material. So, in order to study voids, machined holes are placed in the material to resemble voids in the material. Studying how these voids react is very important, because there are always new inventions coming out that need to conserve material, weight, and cost while maximizing the materials integrity.

Because unexpected results are always a possibility, it is important to be constantly studying how fracture is being introduced into every material through experiments. After reviewing these various papers, I chose to investigate how the hole number and arrangement would change the void growth in 6061-T6 aluminum. The growth of the area of the void is compared to the amount of strain and how it affects the surface in a flat dog-bone shaped sample that has been polished.

Stress-Strain Curve

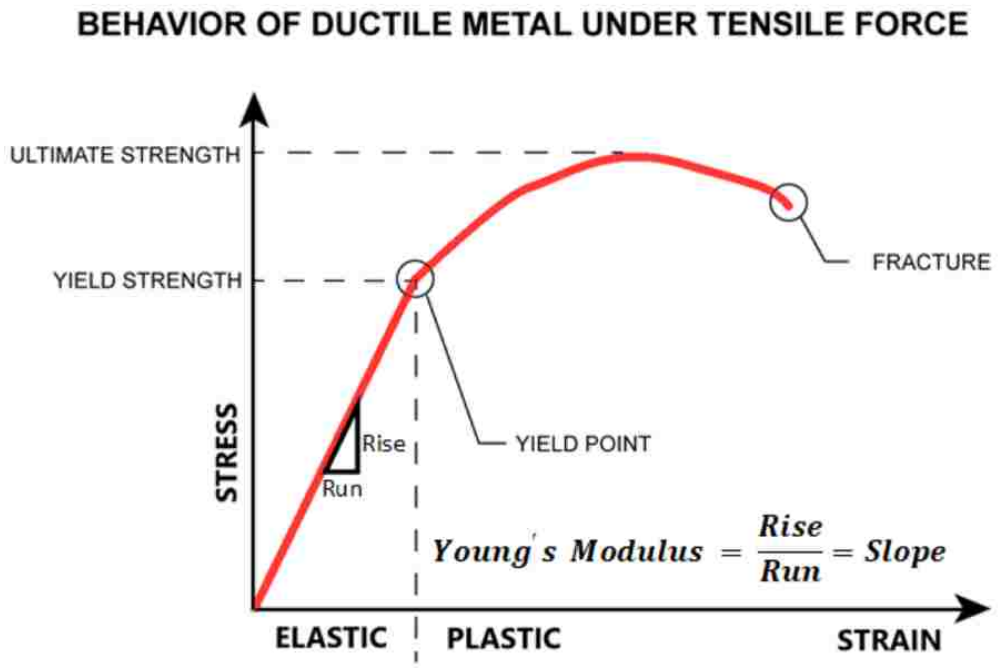

Figure 1 Stress Strain Curve

In order to understand the results of the stress strain curve, we need to know what is going on in Figure 1. This figure is showing how ductile metals behave under tension. The first part of the curve can be called the elastic regime were a material can be stretched to any strain in this section and then released to return back to its original length. The stress in this regime can be directly calculated by using Hooke's Law shown in equation 1.

$$\sigma = E * \varepsilon \qquad (1)$$

In this equation there is a constant E that represents Young's modulus which is unique to different materials and mixtures of material. As you can see in figure 1, the Young's modulus is the slope of the linear portion of the stress-strain curve. The equation also uses ε for strain to solve for stress σ. At the end of the elastic regime there is a point

called the yield point which is the point when the plastic regime starts. The plastic regime is when the sample's strain is so high that when it is released from tension the sample will not return to its original length. This new length is based on how much additional strain the sample experiences past the yield point. The stress curve will unload at a linear rate based on the young's modulus.

Void Area vs Strain Plot

While looking at Mulholland et al. (2006) paper, "void growth and interaction experiments: Implications to the optimal straining rate in superplastics forming", we can see that superplastic materials form an exponential curve when plotting a normalized area of a void verse strain. They also show that with adding more voids along the vertical axis the growth rate of the area slows down allowing it to break after a greater displacement. This is because unlike the single hole which focuses the deformation onto a single area it has multiple areas to focus on resulting in the material being able to stretch at multiple points instead of just one.

SEM (Scanning Electron Microscope)

The SEM analysis is a very useful tool in order to look at how a material is acting in the micro scale. This can be almost impossible to do without machinery such as the SEM because it is so small that the naked eye cannot see what is happening. The SEM is also important to use because unlike a normal microscope it does not need a smooth flat surface in order to focus on the sample. This is very important because after any plastic deformation, the sample will lose its smooth polished finish as it necks. The SEM works by shooting a focused electron beam at the sample creating a picture of the

surface at a certain magnification. The electrons react with the materials on the surface giving different diffractions so that the image shows different levels.

AFM (Atomic Force Microscope)

When looking in more depth into the part from the SEM, a nano scale analysis needs to be performed using an AFM. The AFM is one kind of SPM (scanning probe microscope) that is designed to measure local properties. These local properties consist of things like height, friction, and magnetism as the probe scratches across the surface of the part. This probe is an atomic needle that the AFM scratches across the sample recording all of the different local properties between the needles and the sample. The tip of the needle is normally a 3-6 μm tall pyramid with 15-40 nm end radius (Wenjie, 2003).

Method

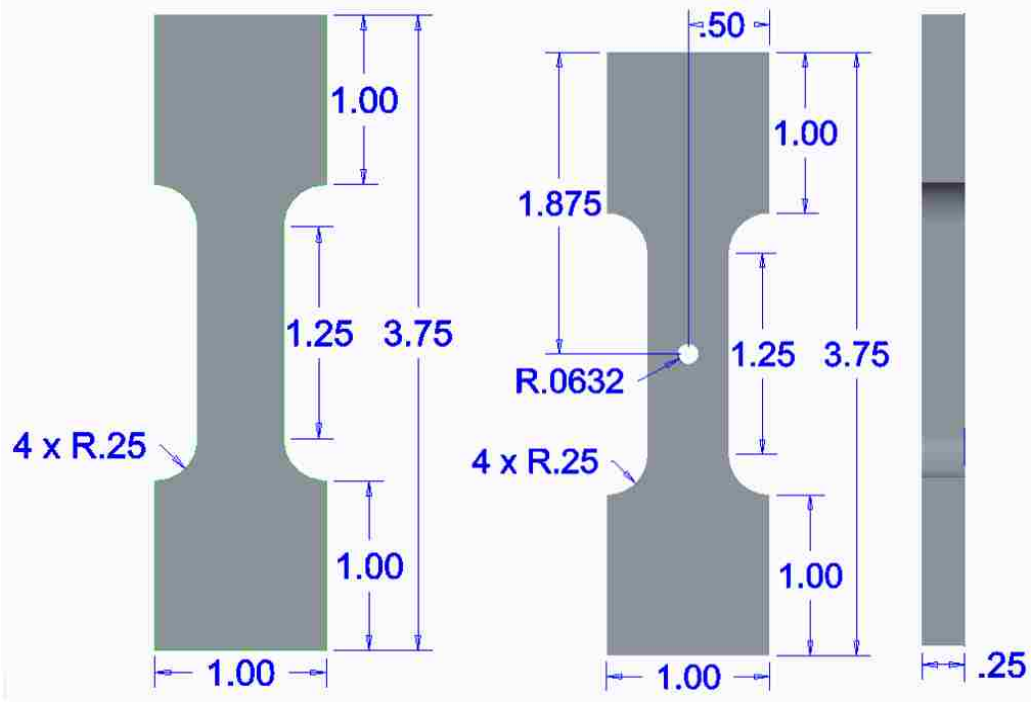

Figure 2 Cad Drawing for samples with no hole and one hole.

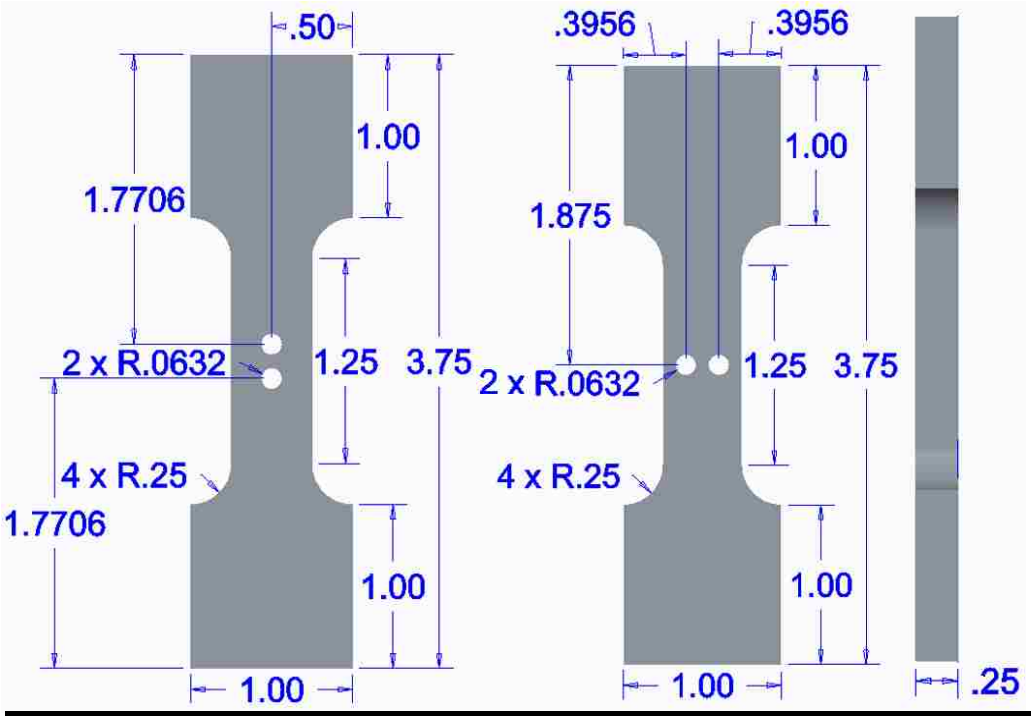

Figure 3 Cad drawings for samples with 2 holes

The dog-bone samples (Figure 2 and 3) were made from two 6ft certified 6061 T6 aluminum flat bars that were ¼ inch thick. These bars were then given to a machinist to cut them into the dog-bone shape using a CNC mill. Once they were cut into their shape, the machinist took a very thin layer of metal off both faces of the sample to prep them for polishing. After all the samples were cut to the same shape and size shown in figure 4, the samples were split into 4 different groups. These groups consisted of no holes in the sample, one hole in the center of the sample, two horizontal holes at the center of the part, and lastly two vertical holes in the center of the part shown in figure 4.

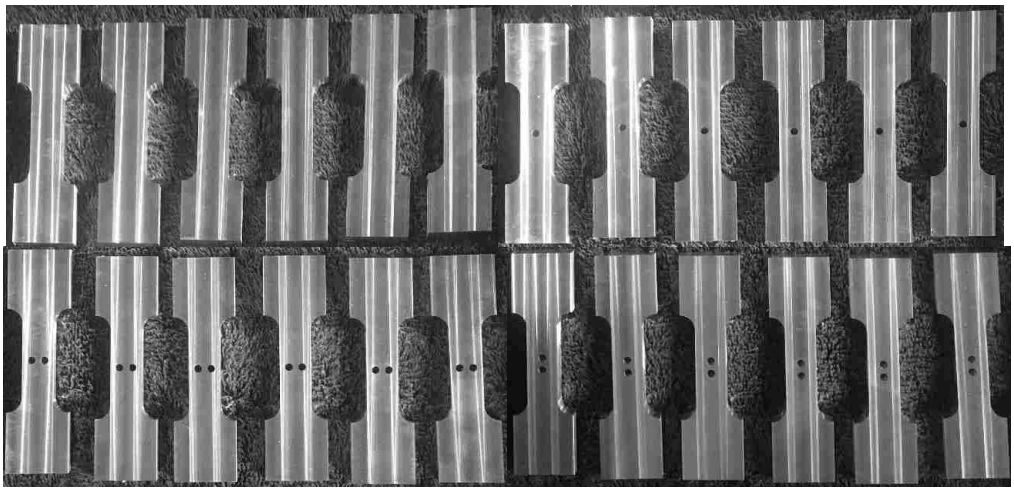

Figure 4 Unfinished samples

These holes were created by drilling and reaming a 1/8-inch hole. Once the parts were cut and drilled, a holder was made in order help keep an even pressure on the samples during the sanding and polishing process as shown in figure 5, 6, and 7.

Figure 5 This is a picture of the holder that was created to hold the samples while they were being sanded and polised. The handels were spread out evenly so that an even amount of pressure can be applied to make the samples as flat as possible.

Figure 6 This is the bottom view of the holder showing where the sample will be held. The depth of the slot used to hold the sample was slightly less than the overall thickness of the samples.

Figure 7 This image is showing a small set screw that was on one end of the holder that was used to pinch the sample into the holder. This was to prevent the sample from having any movement during the sanding and polishing process.

After the holder was created, the samples where sanded using 1000 grit sandpaper on a disk sander for 3 minute each and then rinsed off with water. The parts were then polished on the disk sander with a nylon polishing cloth with plenty of 9-micron diamond paste with diamond extender. The polished samples were then rinsed off and placed into a beaker of deionized water which was then placed in an ultrasonic cleaner for 3 minutes while the next sample was being polished. This process was repeated for 3 microns and 1 micron until the surface was mirror like, as shown in figure 8.

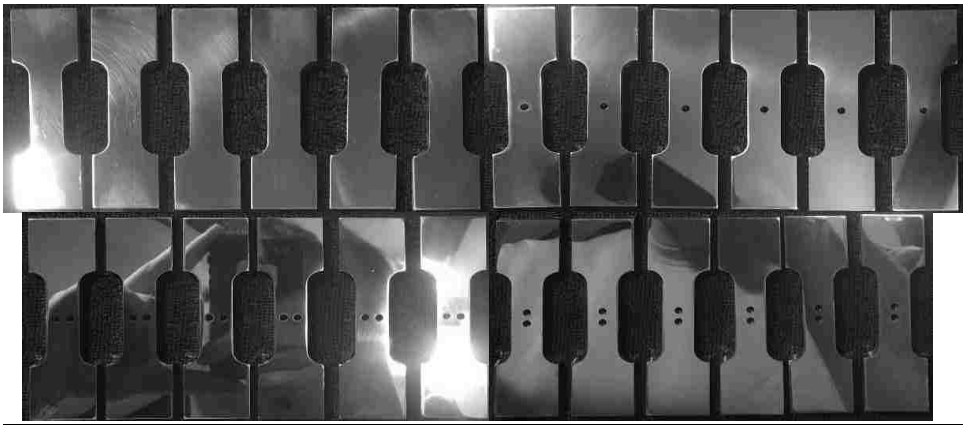

Figure 8 Polished samples

After all the samples were polished, one of the extra samples was etched to calculate the grain size of the material. The etchant that was used was 15 parts HF, 10 parts H_2PO_4, and 60 parts H_2O. This etchant 7 years old so instead of 1 minute to etch the part, 3 minutes was needed to see the grain boundaries. After getting a picture of the grains, we used the circle method to calculate the grain size which resulted in an average size of 129.32 micrometers. This is a very surprising value because the recorded average value that was found has an average of 15 micrometers.

Results

After the samples where polished and ready for testing, they were hooked into a tensile tester. In order to compare the results to what previous results have shown, we did a calculation using the following function

$$\text{Load}_{\text{Max}} = \text{Tensile Strength} * \text{Area} \quad (2)$$

$$\text{Area} = \text{Width} * \text{Thickness} \quad (3)$$

using 45,000 psi for the tensile strength of aluminum 6061-T6 (Kalpakjian and Schmid, 2010). In order to insure that everything is consistent, all the samples were pulled at a rate of 0.01 inches per min. While the samples were being pulled apart, the force and displacement were recorded to make sure that the samples followed a consistent pattern. This was to ensure we have consistent testing.

In addition to multiple tests to ensure the material is uniform, there are multiple samples of various types tested. These include no voids, one voids, two voids horizontal, and two voids vertical.

No Voids

The no voids sample is the standard dog-bone test sample that has been sanded and polished. There was a total of 12 no void samples that were tested. In order to make sure that the material is accurate and the machine is reading the right values, equation 2 was used to calculate the max tensile load. With using the tensile strength of the Aluminum 6061-T6 and the smallest cross-sectional area of the sample we get the following load.

$$\text{Load}_{\text{max}} = 45{,}000\ \frac{\text{lbs}}{\text{in}^2} * (0.5\text{in} * 0.25\text{in}) = 5{,}625\ \text{lbs}$$

The first 6 samples were then used to set up the machine and the video camera. These samples were also used to confirm that we will get value that was calculated with the previously refereed to equation. Once it was confirmed that the values were within an acceptable range of the calculated value and the camera was in a good spot to see the break, the remaining samples were tested and recorded. Three of the remaining samples were pulled all the way past the breaking point, while the other three were pulled to 3 different spots before they broke – yield, ultimate stress, and just before the sample breaks. These three locations where found by using the previous three samples to find an average for yield, ultimate stress, and just before breaking. The results of the test can be seen below.

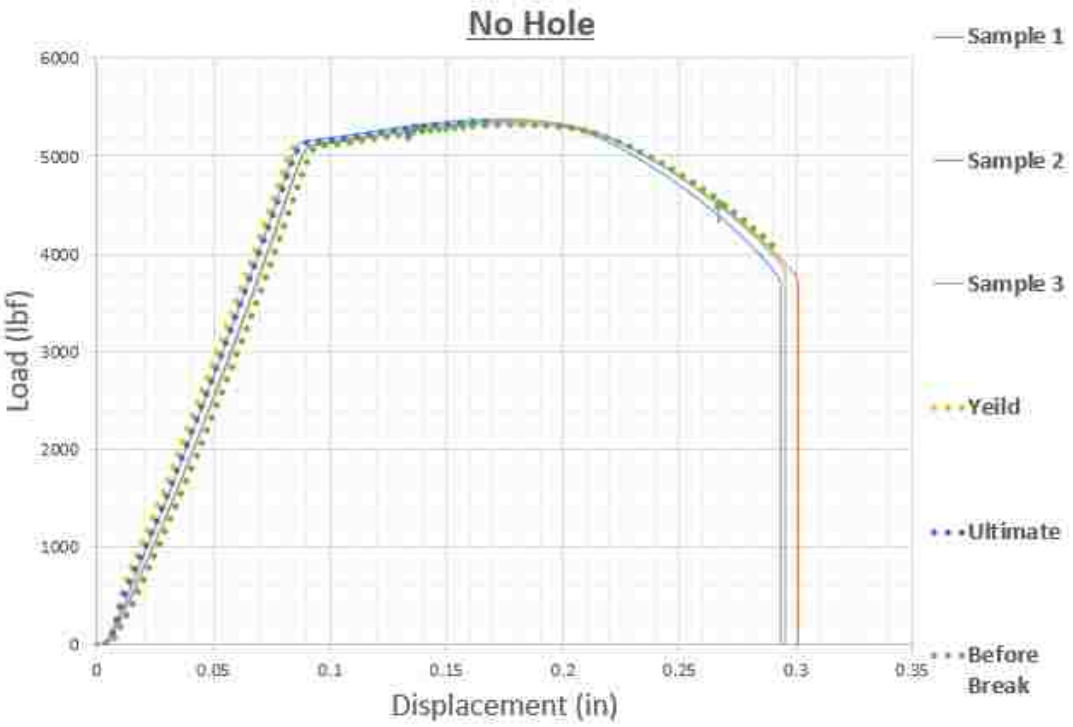

Figure 9 Load vs Displacement graph for samples with no voids

One Void

Because voids can show up in random places throughout the metal, the next 6 samples had a single hole drilled into the center. The single hole is to represent a void in the metal and is large enough for visual observations to be done. This is because a hole acts in the same way a void does and can give us an idea of how a void may act in a material under tension. The hole that was drilled into the part was 1/8 inch in diameter and was place in the exact center of the sample. The reason behind placing the void into the center of the sample was to maintain symmetry. Because the weakest area of the part has now changed to the location of this hole, equation 2 will need to be used again to make sure the material is verifying previous results. The weakest part will now be where this hole is located so the diameter will need to be subtracted from the width shown below.

$$\text{Load}_{\text{max}} = 45{,}000\ \frac{\text{lbs}}{\text{in}^2} * \big((0.5\text{in} - 0.125\text{in}) * 0.25\text{in}\big) = 4{,}218.75\ \text{lbs}$$

With this value the 3 initial tests were run to completion gathering the information so that we can find yield, ultimate stress, and the point just before breaking. These results were then placed in the same graph to make sure they follow a similar path shown below.

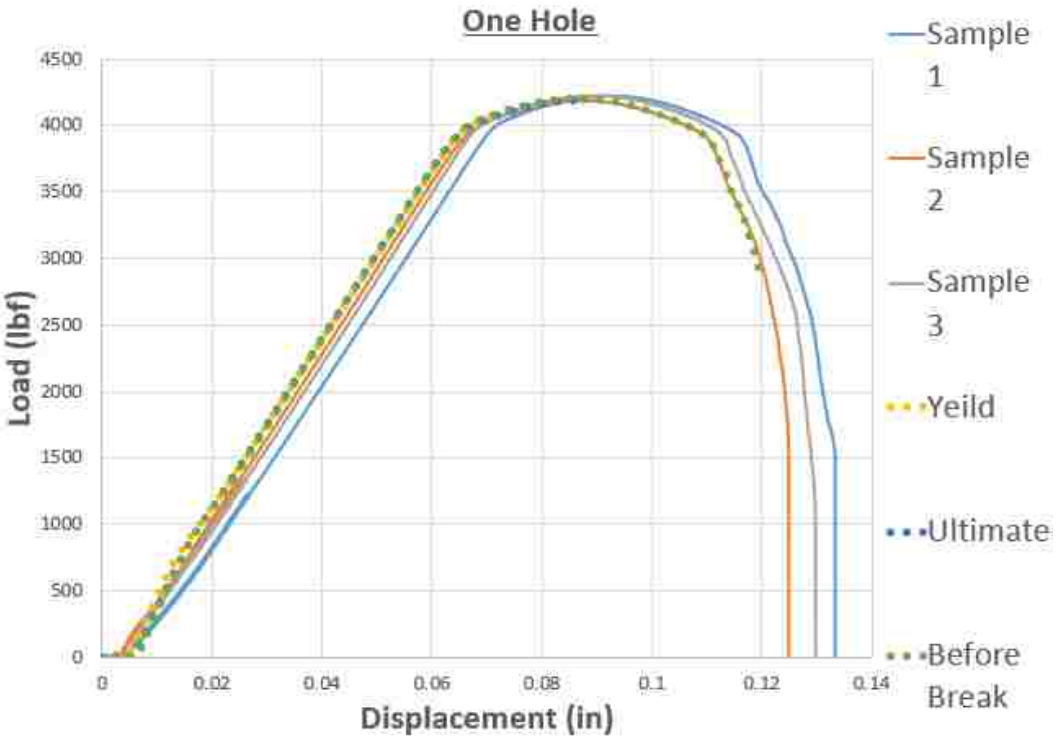

Figure 10 Load vs Displacement for single-hole samples

This void caused the sample to localize the stretch that it was experiencing making shear banding easily visible. Shear banding is where a material that is experiencing extreme strain has plastic deformation that can form a visible line or x in the direction the part will fail. This is shown in figure 11.

Figure 11 Angled picture of one hole sample showing shear banding X forming.

Two Voids Vertical

Now that we had the results for having just one void in the material we wanted to look into what would happen to the stress strain curve with 2 holes in the sample. The first one that we were interested in was the case were you would have two voids spaced vertically along the center of the sample for symmetry. This would have the same weakest point because the smallest cross-sectional area will not change in this experiment so equation 2 will not be recalculated giving the same max load shown below.

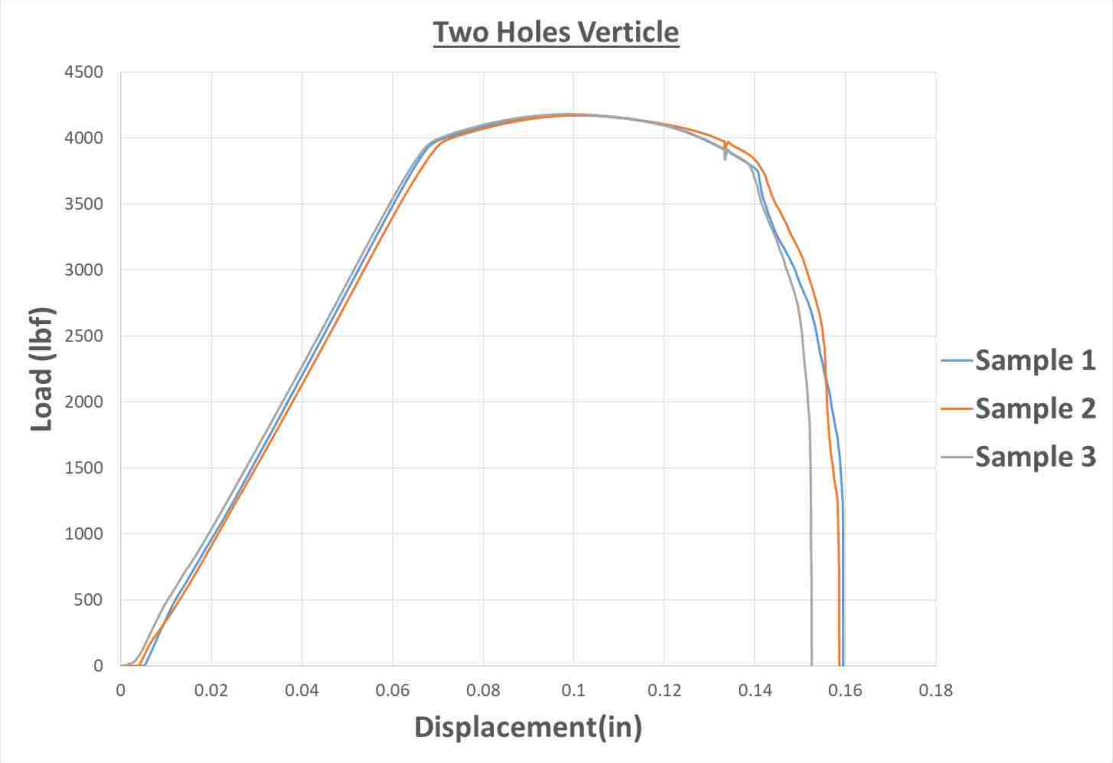

Figure 12 Load vs Displacement graph for samples with two voids vertically spaced.

From this we can see that the maximum load that the sample experiences is the same or similar to the one hole test. However, the sample stretched farther than the one hole. This is because with having multiple holes the sample initially had two areas to localize the stretching creating a double shear banding x pattern before breaking as shown in figure 13.

Figure 13 Double Shear banding picture of two vertical void sample.

Two Voids Horizontal

The last type of experiment that was done to the dog-bone sample was having two holes horizontally spaced. With having the two holes spaced side-by-side, the cross-sectional area of the parts will be reduced by an additional hole diameter. This change will require another calculation by equation 2.

$$\text{Load}_{\text{max}} = 45{,}000\ \frac{\text{lbs}}{\text{in}^2} * \left((0.5\text{in} - 2 * 0.125\text{in}) * 0.25\text{in}\right) = 2{,}812.5\ \text{lbs}$$

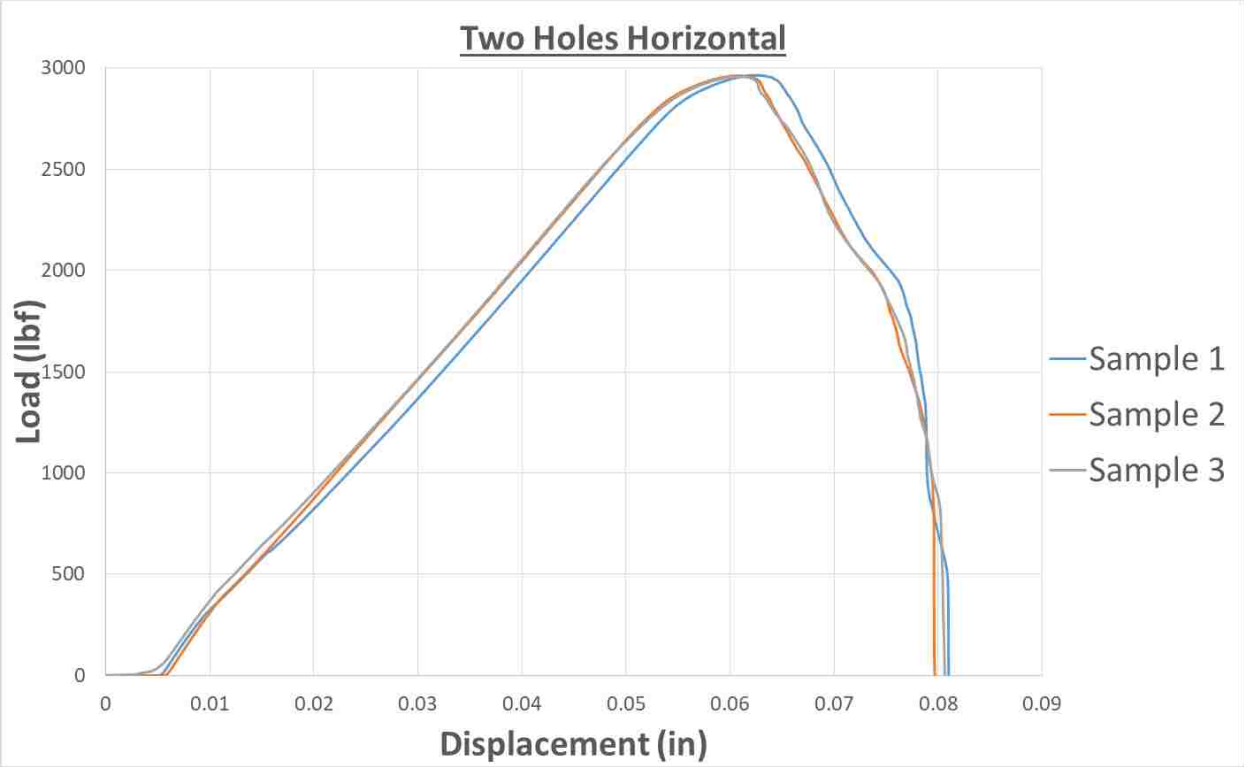

Figure 14 Load vs Displacement for two voids equally spaced horizontally.

Stress Distributions around a hole

When looking into how the void grows, it is important to understand how the stress is being concentrated around the void. Using equations 4-6 we can see how the hole is affecting the different components of stress around it. The variables in these equations are represented in figure 15. These equations are based on having two assumptions, one of these assumptions is that the deformation is small, i.e. elastic, while the other is that the hole is in a plate with an infinite width. Because we cannot have a plate with an infinite width these equations will not give us an exact value, but it can give us a good approximation. These equations were found in (Khraishi, 2013).

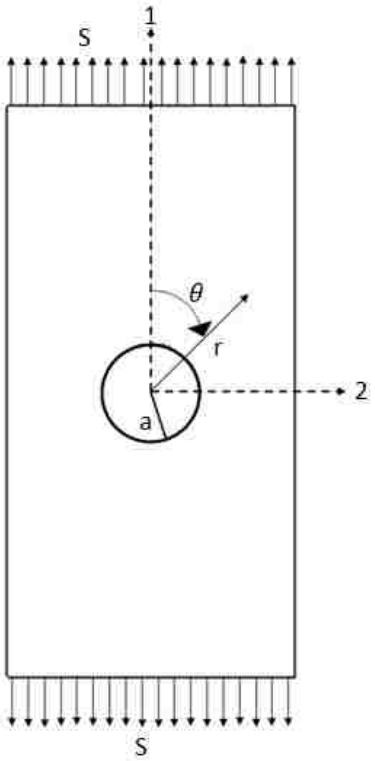

Figure 15 Loading configuration scheme for one hole sample.

$$\sigma_{rr} = \frac{S}{2}\left(1 - \frac{a^2}{r^2}\right) + \frac{S}{2}\left(1 + \frac{3a^4}{r^4} - \frac{4a^2}{r^2}\right)\cos(2\theta) \quad (4)$$

$$\sigma_{\theta\theta} = \frac{S}{2}\left(1 + \frac{a^2}{r^2}\right) - \frac{S}{2}\left(1 + \frac{3a^4}{r^4}\right)\cos(2\theta) \quad (5)$$

$$\sigma_{r\theta} = -\frac{S}{2}\left(1 - \frac{3a^4}{r^4} + \frac{2a^2}{r^2}\right)\sin(2\theta) \quad (6)$$

$$K_T = \frac{\sigma_{11}}{S} \quad (7)$$

These equations will aid us to see if the stress concentration factor is being affected when there are multiple holes in the sample. Later on, these equations will be used to show how the stress is being changed by the different hole formations on the sample parts.

Void Area Calculations

In order to see how the void is changing under the tensile test, we started by looking at how the area is changing with strain. A video was taken straight in front of the one-hole sample during the tensile test. This video was started at the same time the test started so that multiple pictures could be created to calculate the area of the void using particle counting (ImageJ Software). While particle counting is not an exact science, it can give us a general idea of how the area of the hole or void changes during tension test. It was decided to take a picture at the beginning of the video and use a program called imageJ to see how many pixels the void contained. With knowing what the original radius of the void is, we can calculate the area using πr^2 then dividing that value by the number of pixels. A picture was then taken at multiple points throughout the straining process as well as right before it broke. All pictures were processed through imageJ.

One Void

Before looking at how the void is growing, it is important to look at why the void is growing. This is because of the stress concentration around the hole which is shown in equations 4-6. From equations 4-6, we will look at how the stress is being concentrated in a flat plane directly to the sides shown in figure 16.

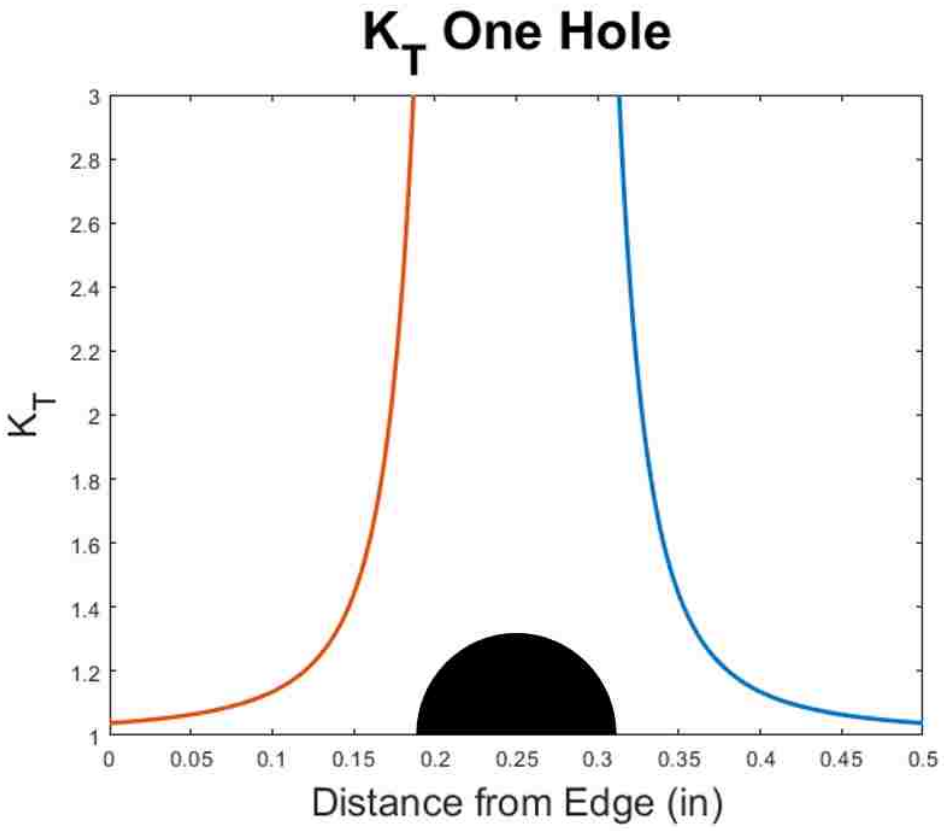

Figure 16 Stress concentration factor for σ_{11} for section directly to the right and left of the hole.

When looking at all of the different stress concentration factors around the hole, it can be seen that the main stress concentration around the hole is the stress in the $\sigma_{\theta\theta}$ direction. From this, we can see that right at the hole the stress concentration factor is 3 while the stress in the sample away from the hole experiences a stress concentration factor of 1.

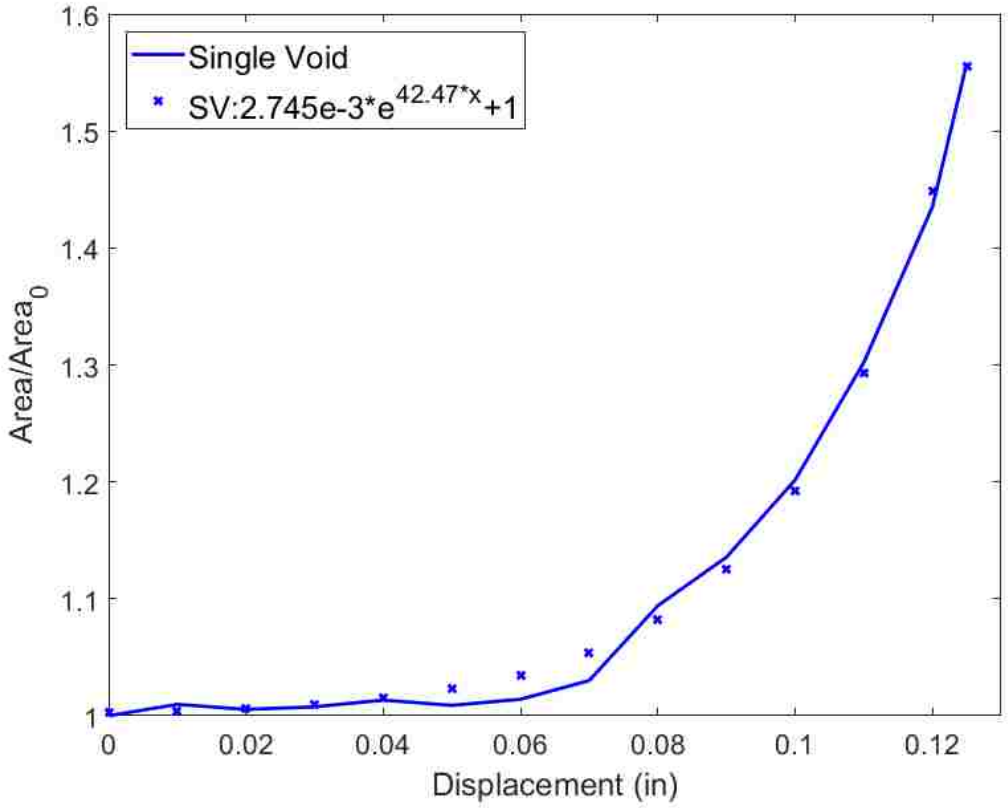

Figure 17 Area vs Displacement for one hole sample.

Similar to the work (Khraishi et al., 2001) did in studying the void area growth for superplastic materials, we can see that the growth follows an exponential growth pattern.

Two Voids Vertical

While it might seem that the stress in the horizontal direction would be the exact same at the one-hole sample, that assumption could not be more wrong. When looking at the stresses, we can see that they are all based on an angle from the hole so each of the holes will have some affect as you can see in figure 18.

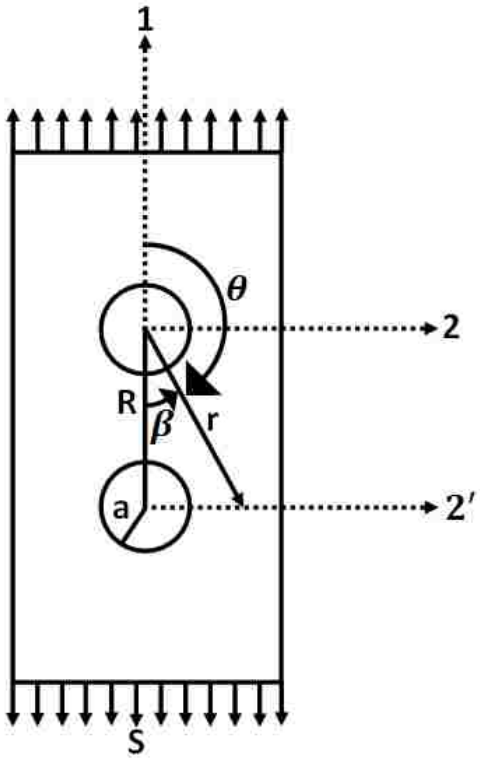

Figure 18 Loading configuration schematic for two hole vertically spaced sample.

From this diagram it can be seen that the existence of the top hole will affect the σ_{11} values of the bottom hole along the dotted line 2`. The derivation of this superposed stress can be found in APPENDIX A. With this superposition we can find a new stress concentration shown in figure 19.

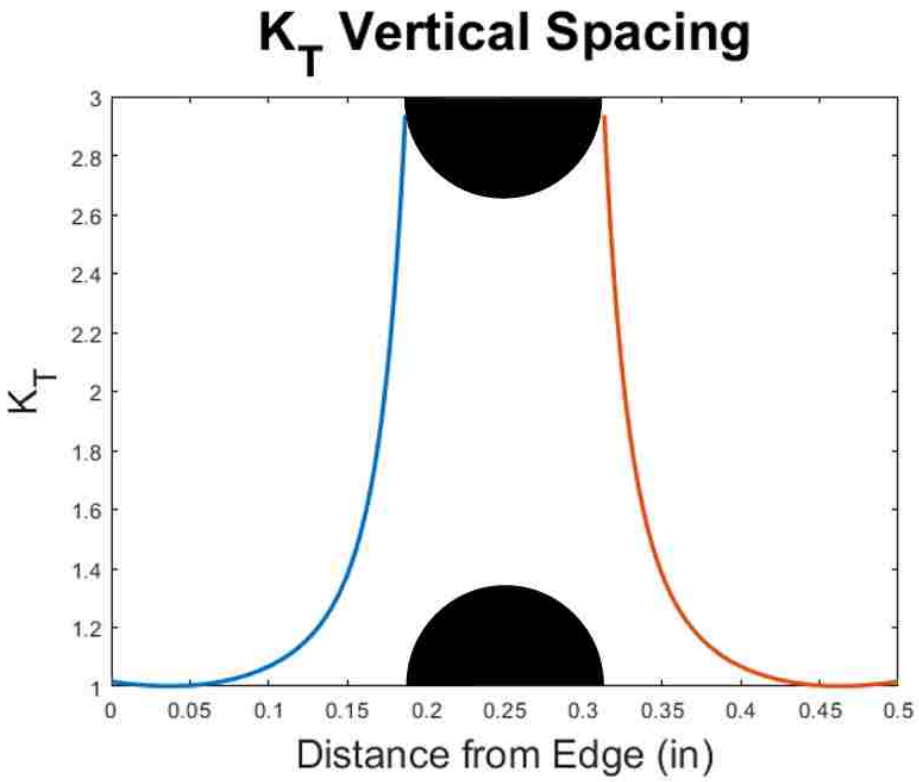

Figure 19 Stress concentration factor for σ_{11} for section directly to the right and left of the bottom hole.

When looking at the stress that the sample is experiencing from having two holes vertically spaced, we can see that the stress in the 1-direction is slightly less than the stress with only one hole. Because of the reduced stress levels, we can expect that the deformation of the holes will be noticeably slower. This slower deformation will cause the voids growth to be delayed as seen in figure 20 when compared to figure 17 which had only one hole. This deformation can only be compared when the area of the hole is normalized.

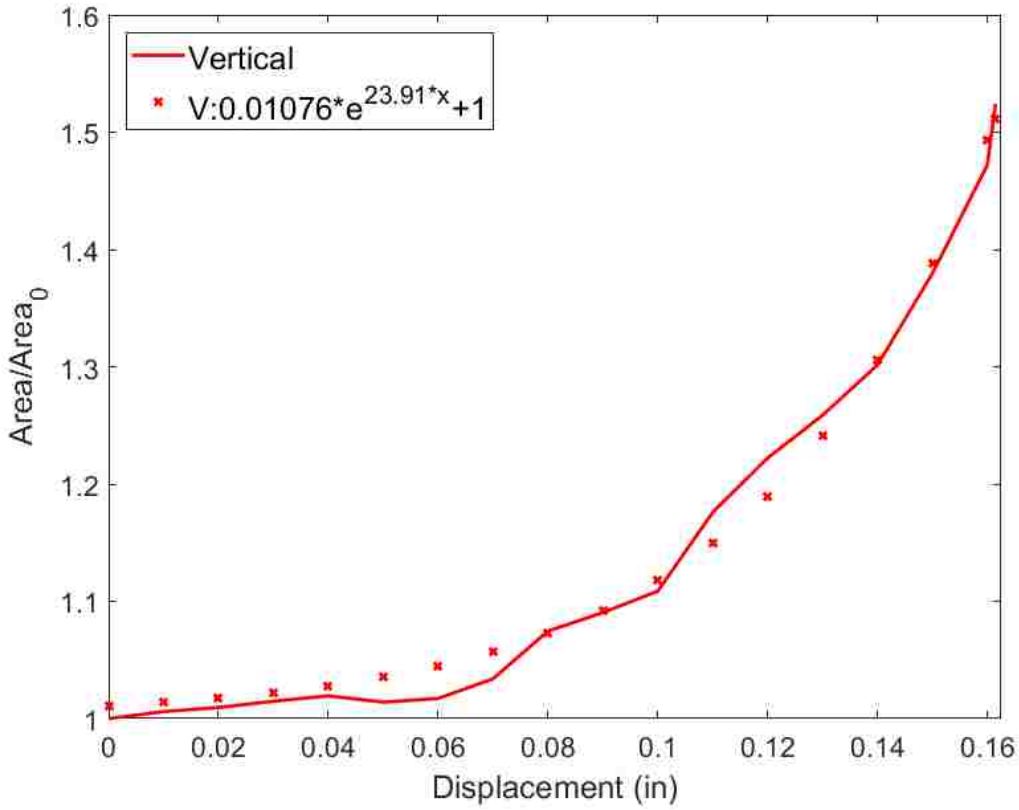

Figure 20 Area vs Displacement for samples with two voids vertically spaced.

Two Voids Horizontal

Now that we know what will happen when there are two holes vertically spaced, it is important to check how two holes horizontally change the void growth. This will change the stress concentration horizontally and if the holes are not far enough apart it will cause the void growth to happen sooner.

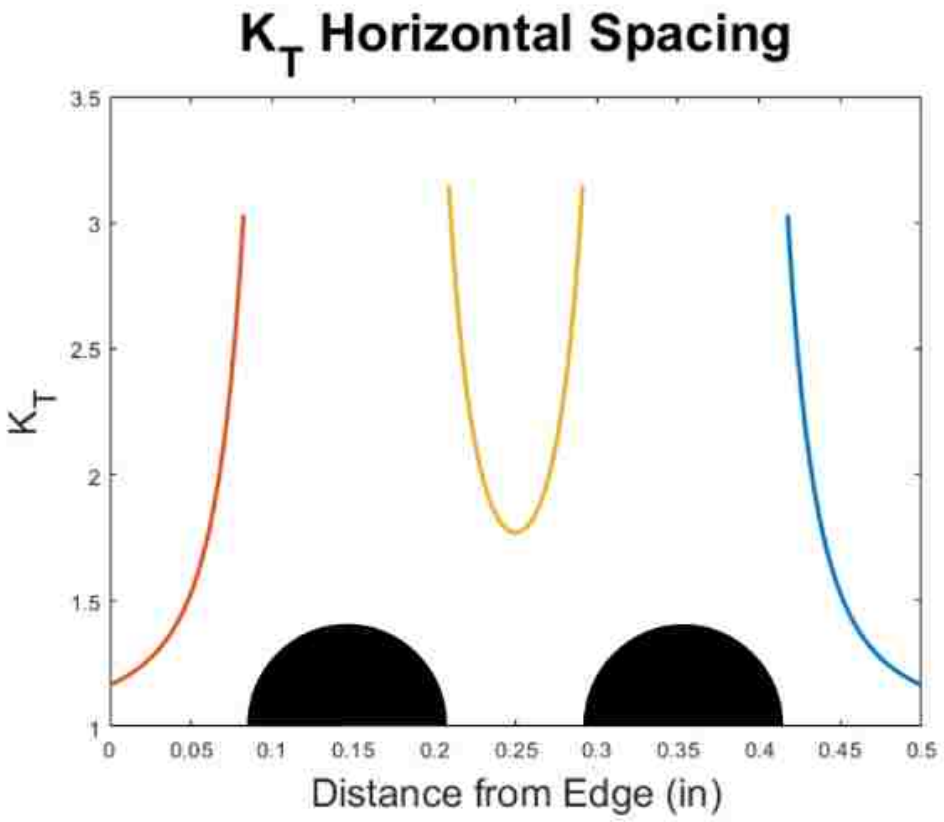

Figure 21 Stress concentration factor for σ_{11} direction. The x axis is strating at the left edge of the sample. The orange line is the factor to the left of the holes, yellow being the stress concentraion fractor between the holes, and the blue is the factor to the right of both holes.

With looking at figure 21, you can see that the stress is slightly affected by having the two holes. The major contributing stress factor, σ_{11}, seems to only have a small increase in the maximum stress around the inner edge of the hole that changed to 3.15 instead of 3. The elevated stress values between the holes is expected to drive faster hole growth. This growth can be seen in figure 22 compared to the growth in figure 17.

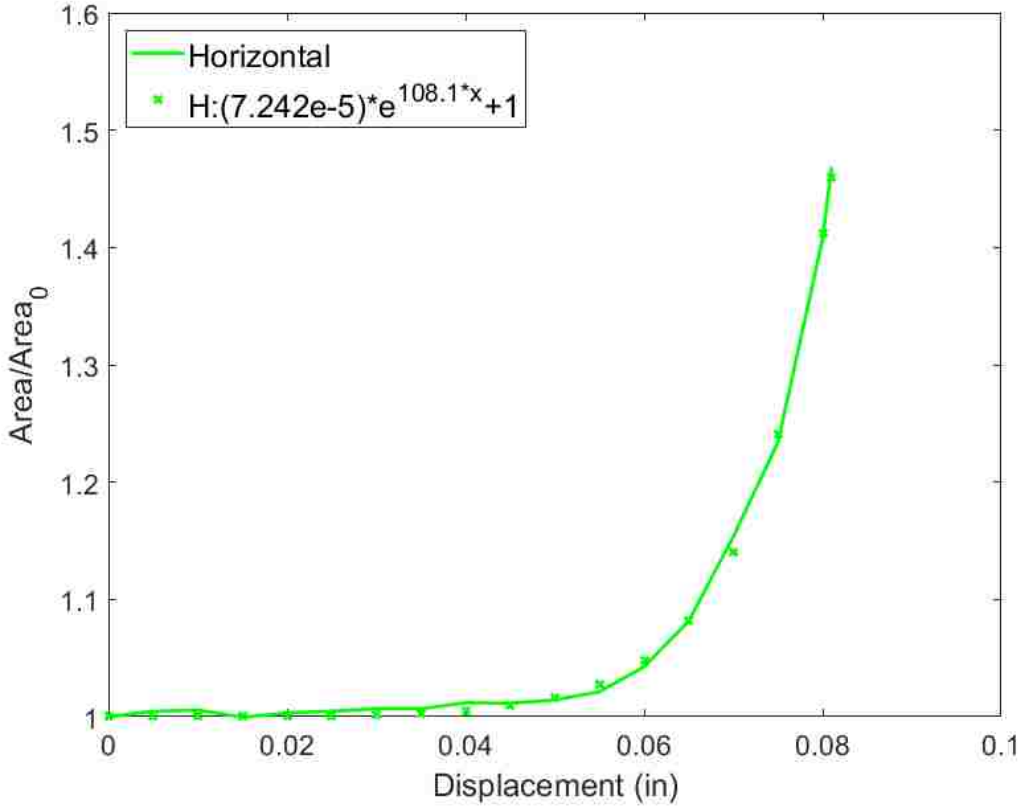

Figure 22 Area vs Displacement for samples with two voids horizontal.

Comparing Void Growth

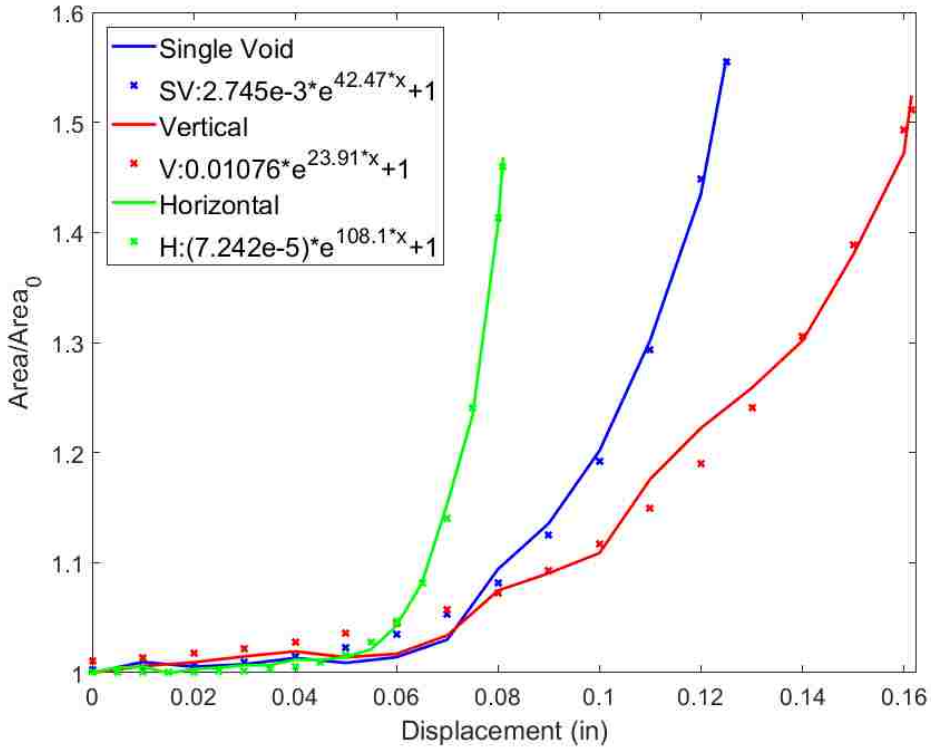

Figure 23 Normalized area vs Displacement for all three samples along with an exponential curve fit for each of the samples.

When comparing the results from the one hole and the two-hole tests, we can see that the increase in all three samples follows an exponential growth. From these exponential equations, we can see that the major difference between the three equations is the exponent used for each one. The exponential growth starts at different times for each type of sample tested with the one-hole sample starting between the two different two-hole samples. With using the one-hole sample as the base for comparing the three growth rates, we can see that the vertically spaced holes has a lower exponent and the horizontal has a larger exponent. The reason for the two vertical holes taking longer is due to the fact that each of the holes were experiencing the growth at the same time along

with the decreased stress concentration between the holes. The two horizontal holes curve has a larger exponent because the stress is more concentrated in the horizontal direction. This increased stress causes the part to deform earlier than the one-hole sample. Although this is slightly different than what (Khraishi et al., 2001) did when they considered how the changing in the size of the void would affect the growth of the normalized area, we can still see similar behavior. They saw that when they increase a void's cross-sectional area the exponential growth of the voids area occurred at a more rapid rate. Similarly, it can be seen that when the cross sectional area doubles, it affects the void growth in the same manner as when the two voids are spaced out horizontally.

SEM Results

The samples where polished down to 1 micron to give a mirror like finish so that after the samples where pulled to just before breaking we could observe how the surface is changing. The polishing cleans any surface the parts may have that are not a result of the testing being done. The polishing is also done so that we know how the test is changing the sample's surface while it is necking during the pulling.

We decided to use a Scanning Electron Microscope, SEM, rather than a traditional microscope, because after the tensile pulling the surface would no longer be smooth and observing all the various surface changes with a traditional microscope would be very difficult to impossible. Microscopes don't have much depth vision, while the SEM takes a picture that shows all the hills and valleys left in the part after being pulled to just the breaking point.

Bottom

Looking at just below the void of the sample, we can see that there is no slip or movement in the grains on the surface showing that no deformation has occurred (figure 24). This is due to the hole localizing the stress and strain on the sample during tension. This means that it is focusing all of the dislocations in the material on the sides of the hole leaving the top and bottom unaltered like shown in Ray's Thesis (2003). Although Ray did not have the same shaped sample, we can see in his samples that the bottom of the hole was unaffected just like the top of the hole.

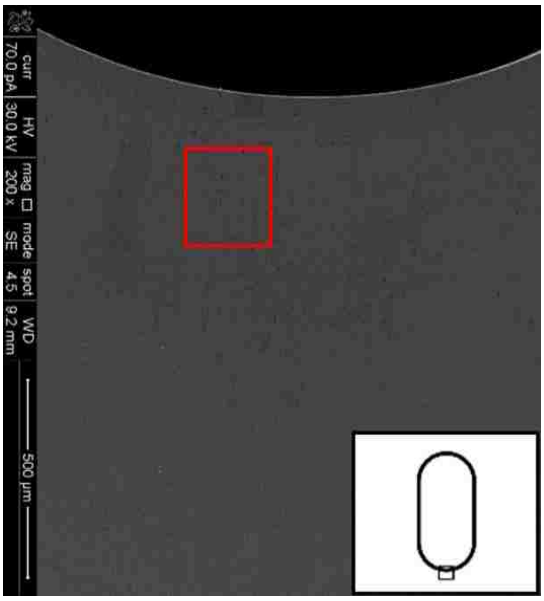

Figure 24 SEM picture of the bottom of the sample after being pulled to just before failure

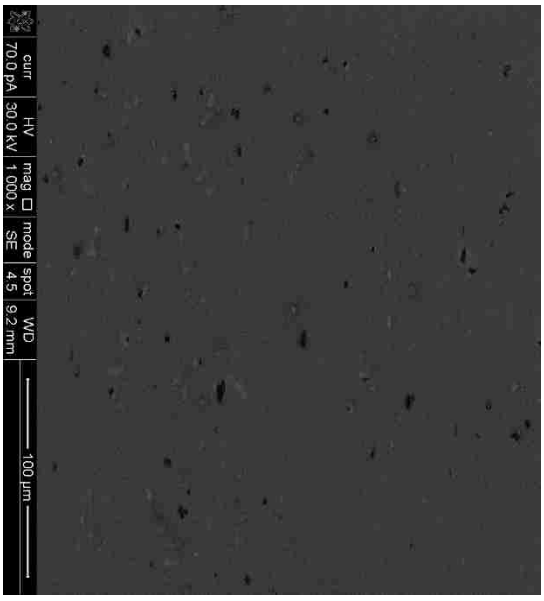

Figure 25 Zoomed area of the red box in figure 24 at 1000x magnification

Bottom Right

Now going around the hole clockwise we will now look at the bottom right. Looking at figure 26, we can see two areas of importance which have been highlighted with two boxes. When looking at the red box, we can see how the edge of the hole is starting to break which will ultimately start a crack for overall breakage. Looking at the yellow box, we can see the shear lines that are caused from the shear banding of the aluminum sample. These shear lines are caused when grains experience extreme local strains. The orientation of the FCC, face center cubic, lattice helps determine the direction of the shear lines (Kalpakjian and Schmid, 2010). Each grain will only have one direction and it will usually be in the direction the sample is likely to break in. Unlike in Ray's thesis where at high tension the grains seemed to almost have completely different direction for the shear banding, we can see that the shear bands are mainly going in the

same overall direction. This can be due to the bending in his sample due to the fact that his samples were not completely flat.

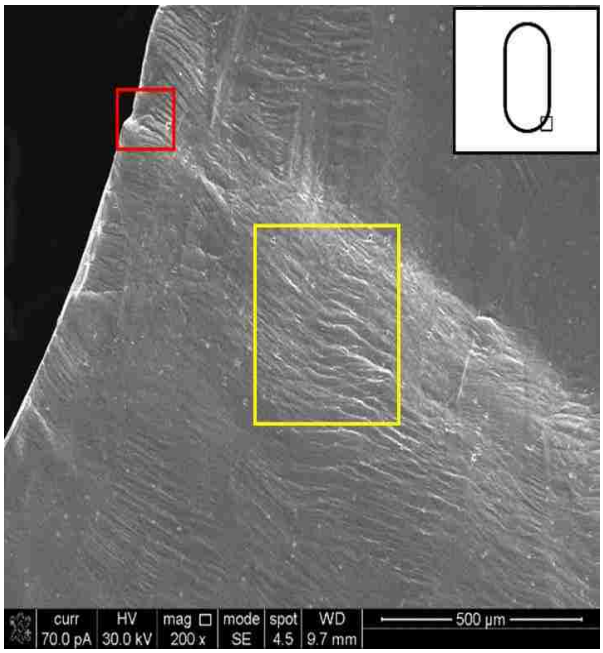

Figure 26 Bottom right corner at 200x

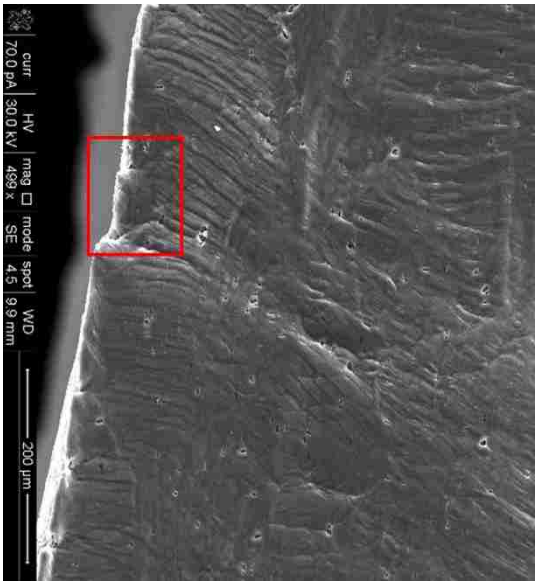

Figure 27 Zoomed in SEM image of the red box in figure 26 at 500x magnification

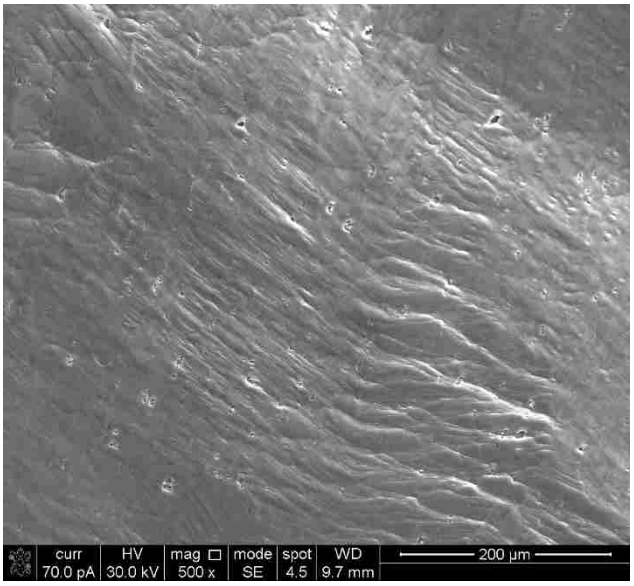

Figure 28 Zoomed in SEM image of the yellow box in figure 26 at 500x magnification

Getting another view of this area that is slightly above the previous, in figure 29 we can see that there is not just one crack on the edge of the hole but two as shown in figure 30.

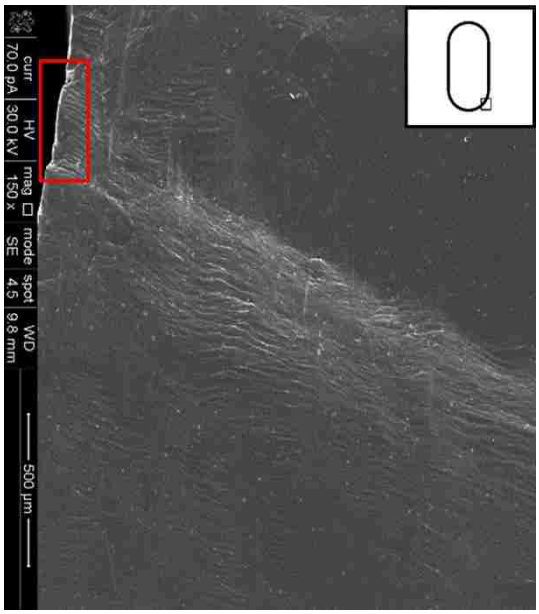

Figure 29 Bottom right corner at 150x magnification

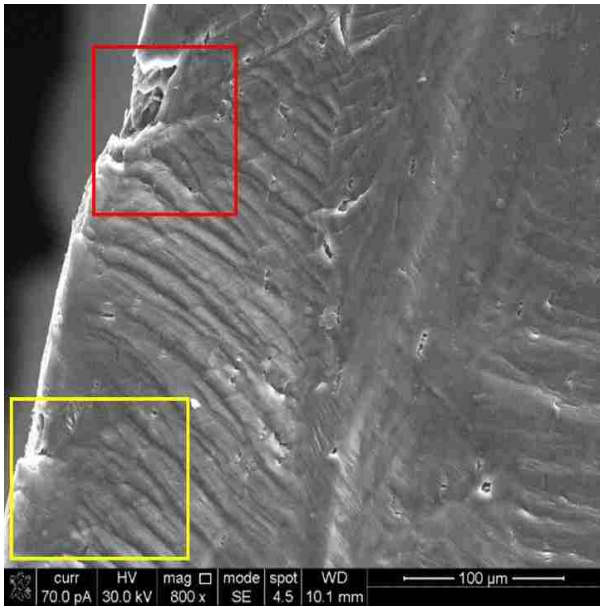

Figure 30 Zoomed in SEM picture of the red box in figure 29.

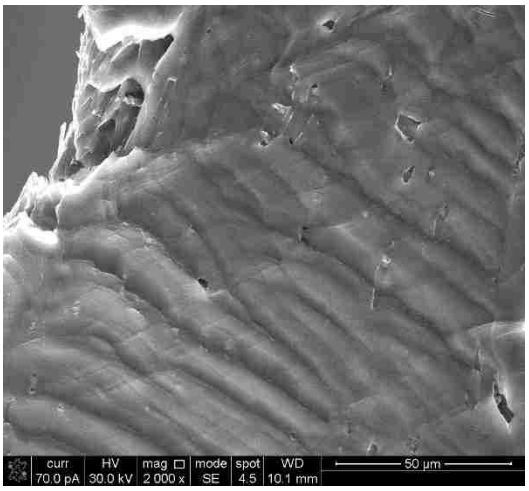

Figure 31 Zoomed in SEM picture of the red box in figure 30.

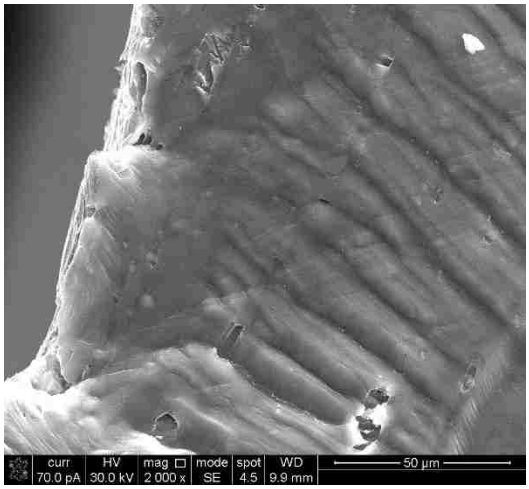

Figure 32 Zoomed in SEM picture of the red box in figure 27 and just below the yellow box in figure 30.

Top Right

Continuing the investigation around the hole look at the upper right area of the shear banding X. It can be seen that on the edge of the hole another break is starting to form in the sample showing that the material is not just showing signs of breaking one direction but in multiple directions.

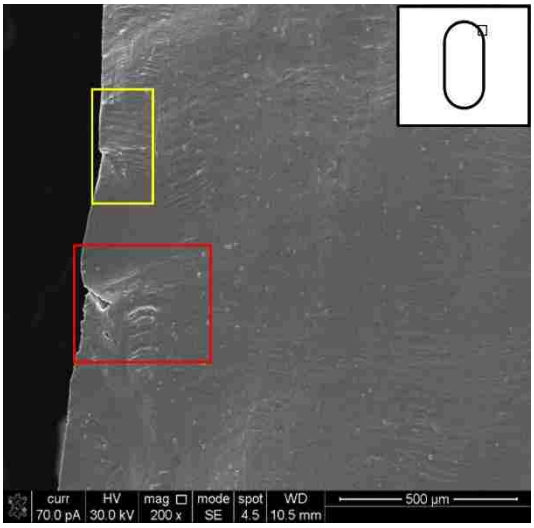

Figure 33 SEM picture of the upper right side of the sample

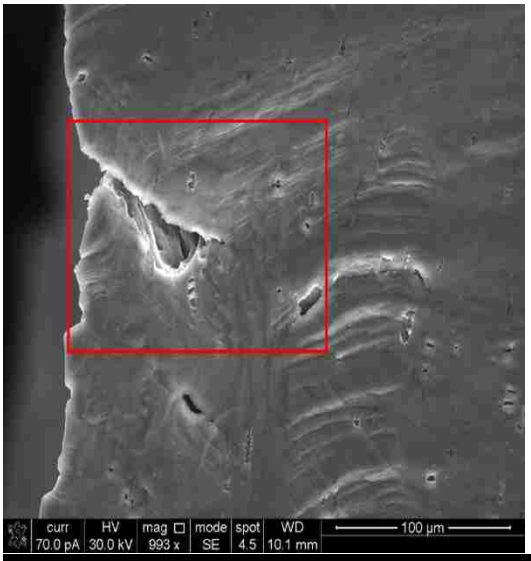

Figure 34 Zoomed in SEM picture of the red box in figure 33 at 1000x magnification.

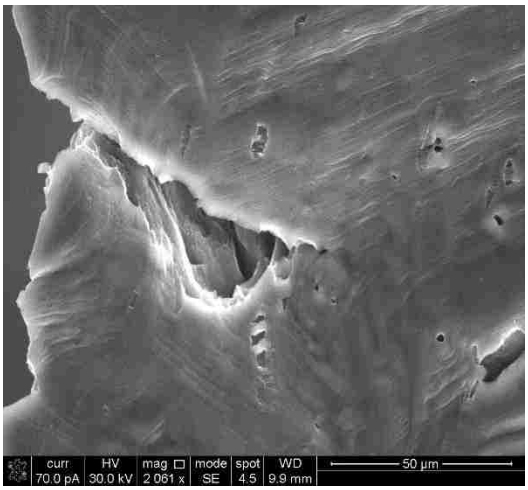

Figure 35 Zoomed in SEM picture of the red box in figure 34 at 2000x magnification.

Continuing to explore the upper right portion of the sample we can see an imperfection in the surface shown in figure 36. This imperfection can be a result of the type of material that is being used, 6061-T6, which is precipitate hardened. The precipitate hardening or aged hardening is when the material is hardened using heat to increase traits such as yield strength in ductile materials. The precipitate hardened material will have smaller more rigid particles to try and reduce dislocations. If these particles or grains do not deform in the material when under tension the grain can break apart causing a void in the material like you can see in figure 41.

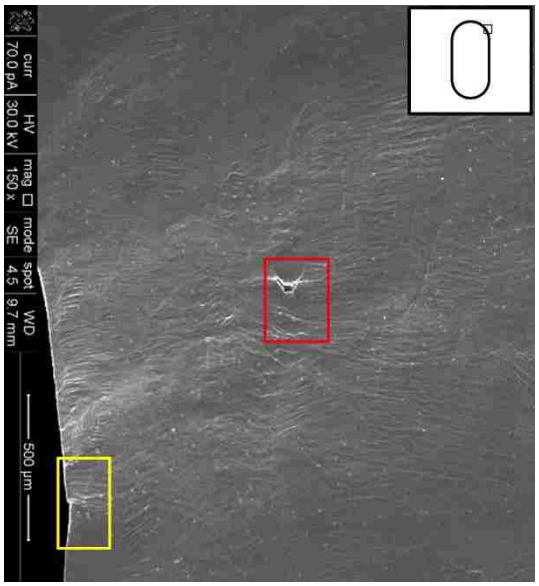

Figure 36 SEM picture of the upper right of the sample just above figure 33. The yellow box in this figure matches the yellow box in figure 33 in order to compare how their locations relate.

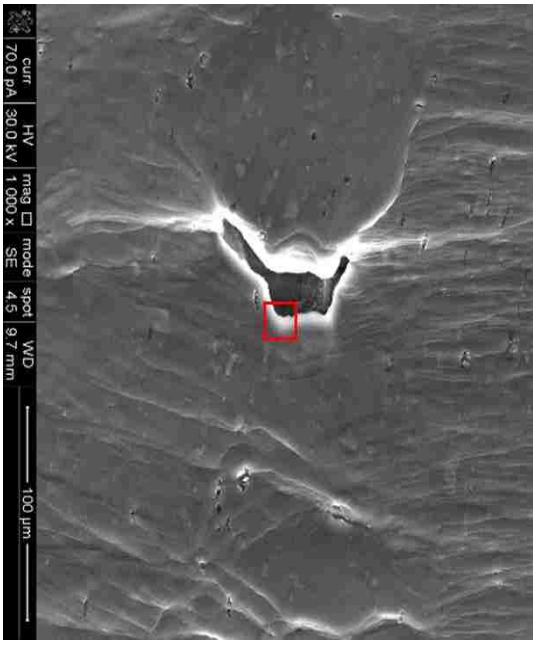

Figure 37 Zoomed in SEM picture of the red box in figure 36 at 1000x magnification.

Figure 38 Zoomed in SEM picture of the red box in figure 37 at 10,000x magnification showing the difference in the surface of the sample and the surface where the grains broke apart.

Top Left

Due to the top showing the same results of being unaffected from the tension like the bottom of the sample the next area of concern is the upper left side of the sample. From this side we can see the shear banding on the edge of the sample from the dislocations under tension in the part in figure 43 and in figure 40, we can see a void forming on the surface. With figure 42, it can be seen how the precipitate hardened grains resist dislocations in the material causing the grain to not have any shear banding while the surrounding grains are experience shear banding.

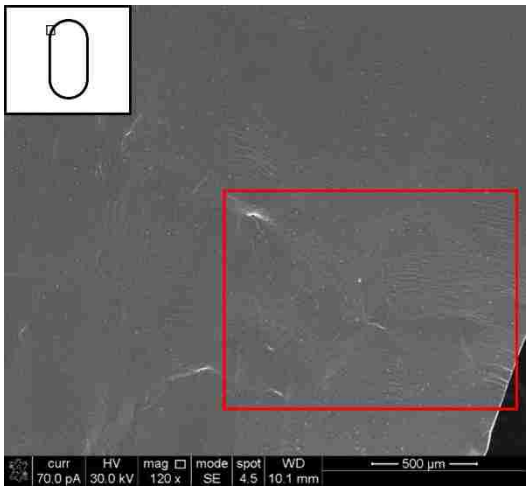

Figure 39 SEM picture of the upper left side of the void

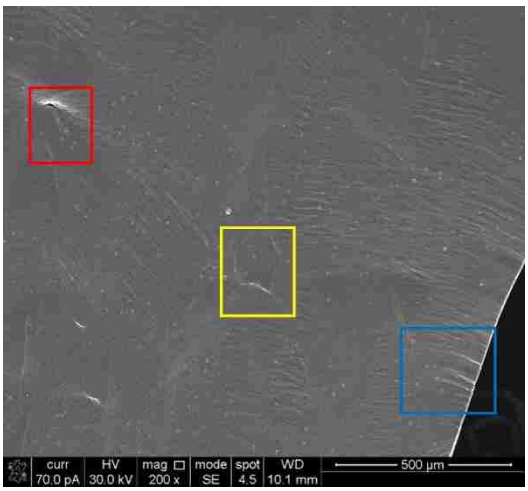

Figure 40 Zoomed in SEM picture of the red box in figure 39 at 200x magnification.

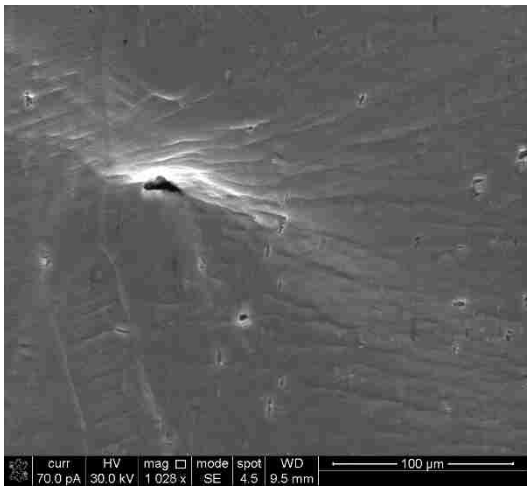

Figure 41 Zoomed in SEM picture of the red box in figure 40 at 1000x maginification. This is showing the start of a void that has grown do the the dislocations in the material.

Figure 42 Zoomed in SEM picture of the yellow box in figure 40 at 1000x magnification. In this picture we can clearly see the outer boundaries of a grain that is resisting the dislocations in the material.

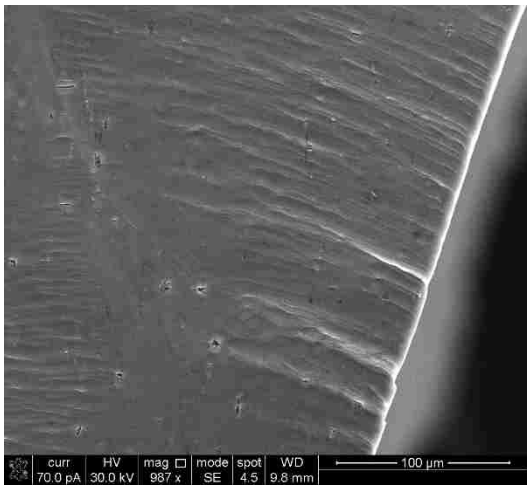

Figure 43 Zoomed in SEM picture of the blue box in figure 40 at 1000 magnification. Here we can clearly see how the material is experiencing dislocations in the material causing a stair stepping look on the edge of the hole.

Middle left

Going down from there we can see more shear banding, voids that are being formed in the material, and more cracks forming on the edge of the hole. From looking at the voids in the sample we can see that the voids follow the direction of the shear banding.

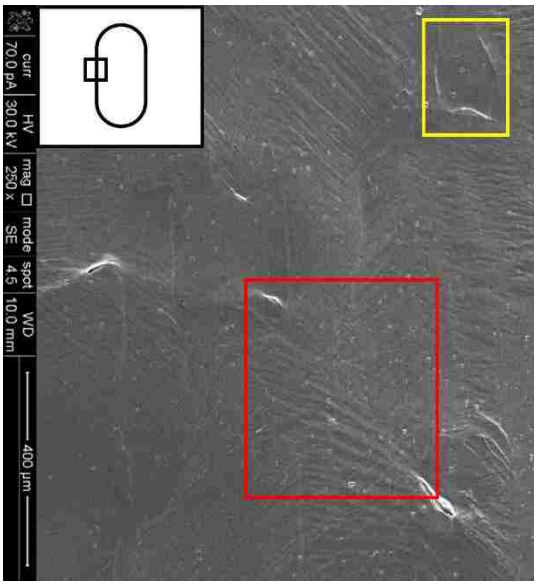

Figure 44 SEM picture of the area just below the top left SEM picture at 250x magnification. The yellow box in this figure is highlighting the same area shown in figure 42.

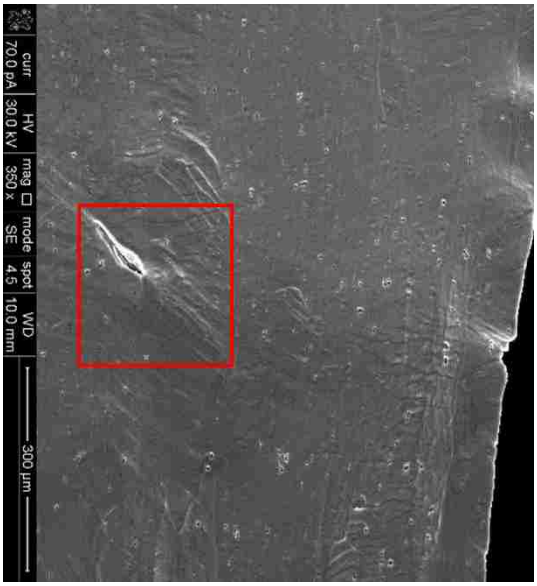

Figure 45 Zoomed in SEM picture of the area just below and to the right of figure 44 at 350x magnification. Here we can see a crack forming on the edge of the hole along with a void forming in the direction of the shear banding.

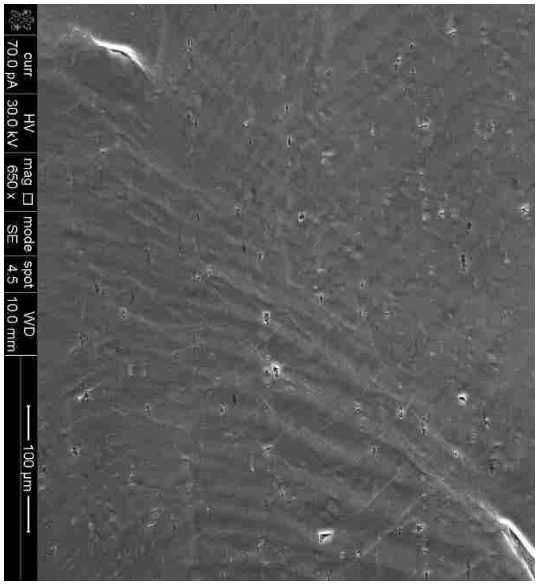

Figure 46 Zoomed in SEM picture of the red box shown in figure 44.

Figure 47 Zoomed in SEM picture of the red box shown in figure 45.

Figure 48 Zoomed in SEM picture of the red box shown in figure 47. This picture is showing us the tip of the void that is being created by the tension. Here we can see that the void is spreading in the direction of the shear banding which will ultimately cas the part to fracture.

Inside Void

After looking at the surface around the hole we look into the center of the hole. In figure 49 we tilted the part 30 degrees in order to see what is happening to the inside surface of the drilled hole. From this angle it looks like the crack has started from the inside of the hole's surface rather than on the edge of the hole where we might expect that all of the stress would be focused.

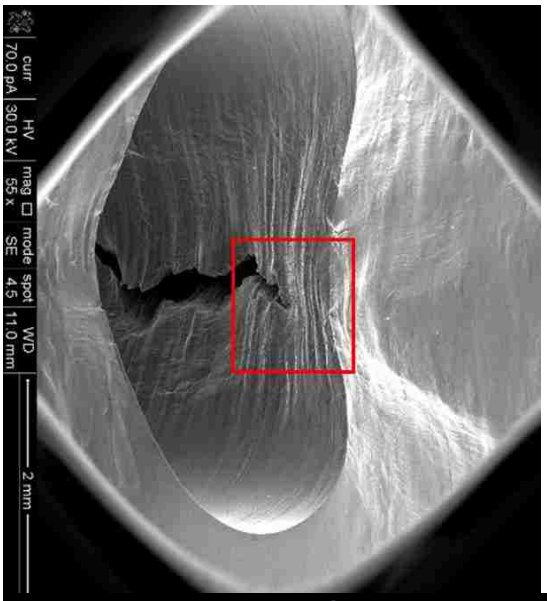

Figure 49 SEM picture of the inside surface on the inside of the hole at 55x magnificaiton. The black sections of the corners of the picture are part of the SEM machine because of how low the magnification is.

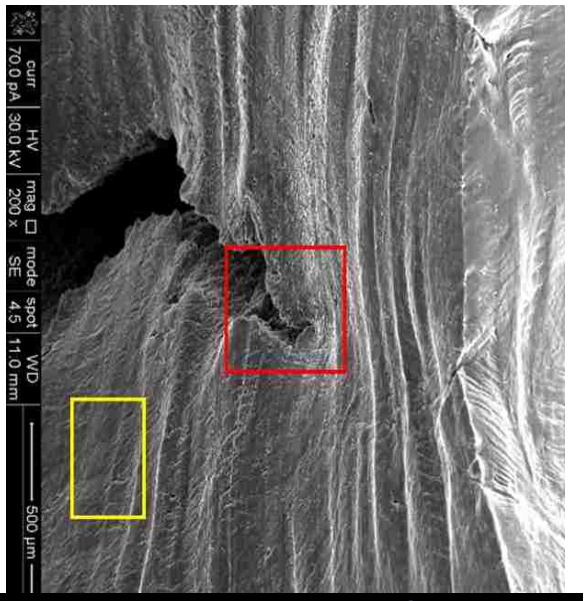

Figure 50 Zoomed in picture of the red box shown in figure 49 at 200x magnification. Here we can see an angled view of the crack that is spreading to the surface causing it to look like the origin of the hole is not the edge.

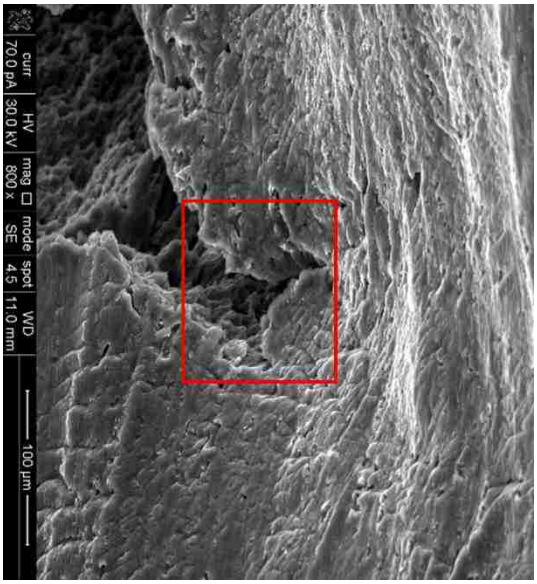

Figure 51 Zoomed in SEM picture of the red box in figure 50 at 800x magnification.

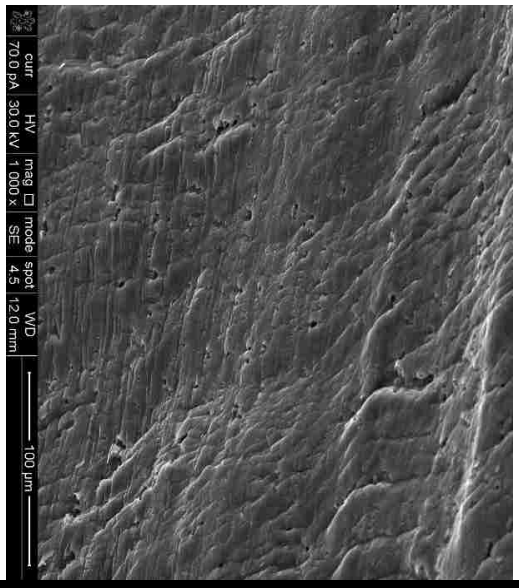

Figure 52 Zoomed in SEM picture of the yellow box in figure 50 at 800x magnification. This image is showing the surface inside the hole. This surface was not polished like the outer surface that we have looked at before this causing it to be difficult to know just what damage was done because of the stretching.

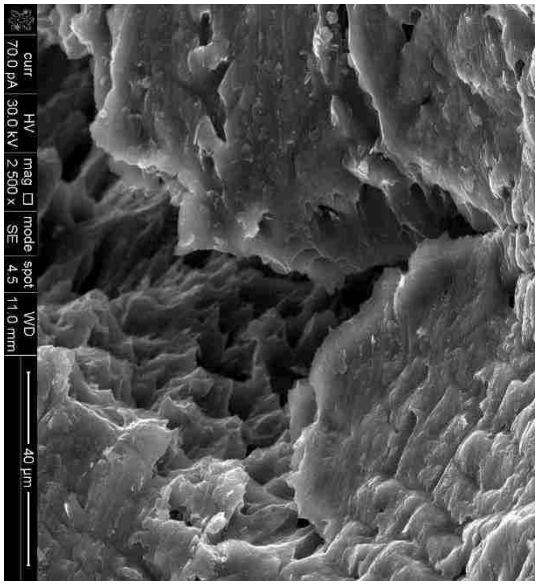

Figure 53 Zoomed in SEM picture of the red box in figure 51 at 2500x magnification.

Through a more thorough search inside the hole, on the surface we can see that on the back edge of the hole a crack has already started to form, shown in figure 51. Due to the fact that we did not have the SEM taking pictures during the pulling process, it is hard to determine if the crack on the back edge of the hole is where this crack started. If this was the case, then the crack on the inside surface of the hole could be showing sign of the crack forming ahead of the original crack like shown in Ray's thesis. The back surface was never polished unlike the front surface giving a rough surface.

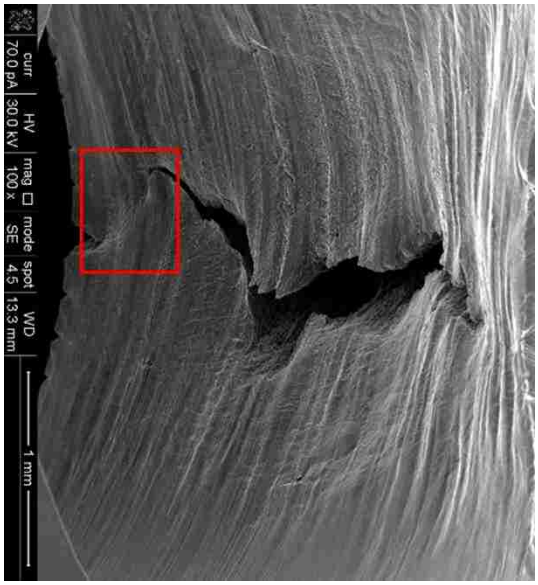

Figure 54 SEM picture of the inside of the hole tilted at a 15 degree angle at 100x magnification. We can see a clear picture of the

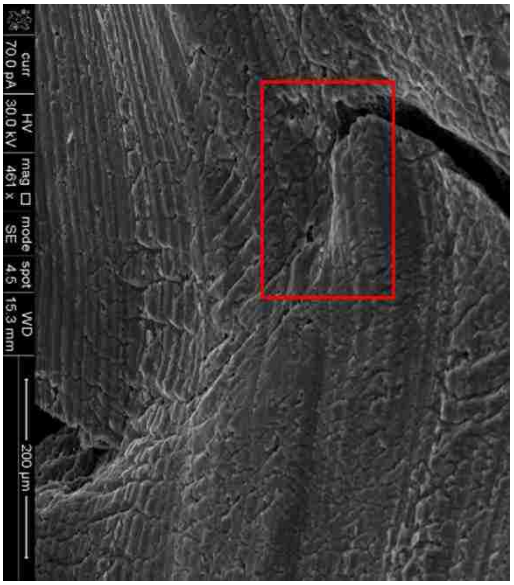

Figure 55 Zoomed in SEM picture of the red box shown in figure 54 at 500x magnification. Here we can see how the dislocations are causing a shear banding that is connecting the two cracks like shown in Ray's paper.

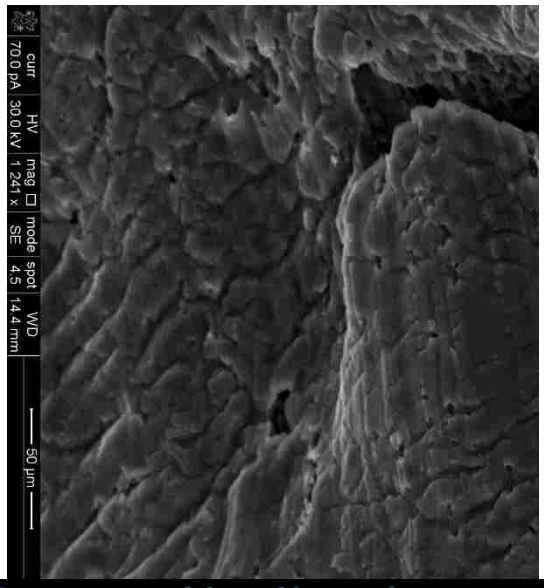

Figure 56 Zoomed in SEM picture of the red box in figure 55 at 1241x magnification. Here we can look at the tip of the crack that is forming and how it is changing angle to follow the dislocations in the material.

Extra

After looking around the hole and inside the hole, some time was spent looking at areas away from the hole to see how the stretching will affect the entire sample. During this investigation we found more shear banding which is to be expected along with an inclusion in the material. Because this material is not one hundred percent aluminum it is easy to see why there will be these kinds of imperfections, shown in figure 58. Imperfections like the one shown in figure 58 can lead to voids when placed under tension which will ultimately coalesce with other imperfection resulting in a crack spreading to failure.

Figure 57 SEM picture showing the shear banding away from the hole in the center of the part.

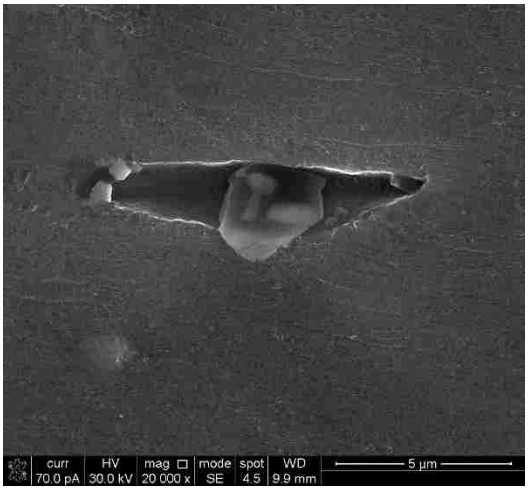

Figure 58 SEM picture of the inclusion found in the samples surface. These types of inclusion can lead to cracks forming and the sample breaking.

AFM Results

The AFM, Atomic Force Microscope, images where collected using a DI-3100 atomic force microscope with a MikroMasch atomic tip. The MikroMasch tips are an n-type silicon material that have an average tip radius of 8 nm. With having the tip at these atomic sizes, we are able to pick up the smallest of imperfection on the surface during the AFM analysis. Due to the small dimples in the material it was decided to use tapping mode to record the surface using AFM. The tapping mode was set to use a frequency of 270 kilo hertz during the scanning process on a 50 micron by 50 micron grid. The resolution that was used for the different samples ranged from 128 x 128 pixel for the smooth sections of the sample to 256 x 256 pixels for the rougher section to capture all of the roughness. The images were taken by Dr. Ezra Bussmann at Sandia National Laboratories on the one hole samples at yield and just before the sample breaks.

The images where then processed through a program called WSxM in order to make sure that the images are showing the same color scale. This program also ran a roughness analysis that gave us RMS, root mean square, roughness (R_q) and average roughness (R_a) so that we can better understand the how the surface change in regard to the stress placed on it. In equations 8-9 we know that Z_j is the Z displacement at each point and N is the number of points within the box cursor. In this program the images were also converted into 3-D plots of the surface so that it is easier to identify the roughness of the surface.

$$R_a = \frac{1}{N}\sum_{j=1}^{N}|Z_j| \tag{8}$$

$$R_q = \sqrt{\frac{\sum_{j=1}^{N} |Z_j^2|}{N}} \quad (9)$$

Yield Sample Results

Polished

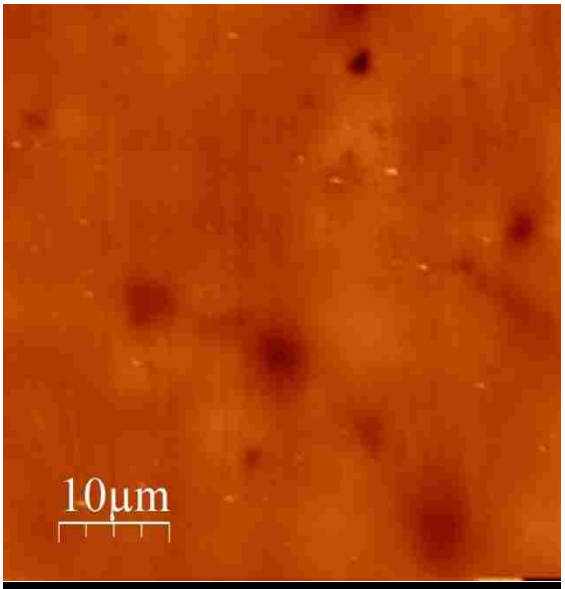

Figure 59 AFM picure of the smooth polished section under the hole for the sample pulled till just after yield.

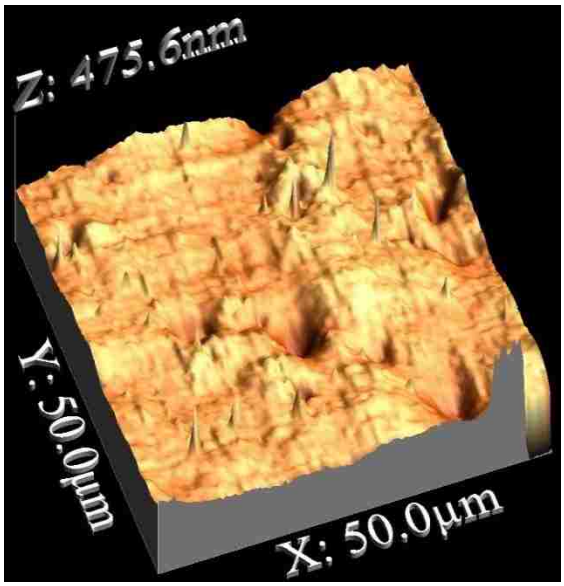

Figure 60 3D image of the surface shown in figure 59.

	RMS roughness	Roughness average
Figure 59,60	24.9873	16.9632

Middle Right Section

When looking that AFM pictures taken from the right of the hole, we can see that as the scanning move closer to the hole the RMS roughness and roughness average on the surface increases. This is to be expected when moving closer to the hole because as the sample stretches the dislocations are going to focus around the hole. When looking at the roughness for the samples that were farther away from the hole, we saw that the

roughness became closer to the polished section. This is because the dislocations in the part are focusing at an angle leaving the section directly to the sides of the hole relatively unaffected.

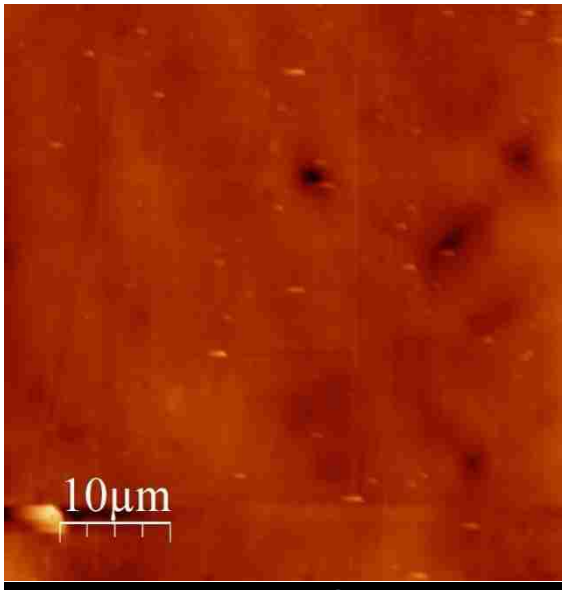

Figure 61 AFM picture of the the area around the middle of the sample about 200 microns to the right of the hole.

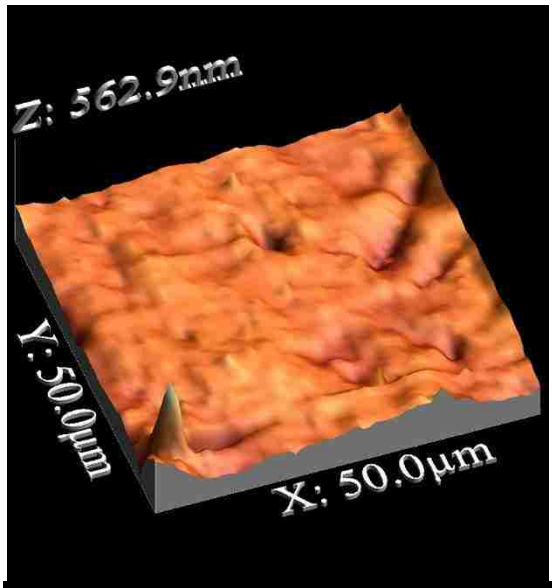

Figure 62 3D image of the surface shown in figure 61.

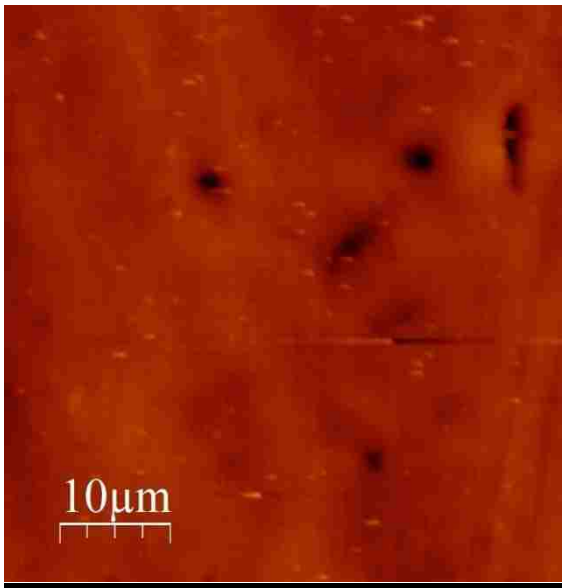

Figure 63 AFM picture of the the area around the middle of the sample about 100 microns to the right of the hole.

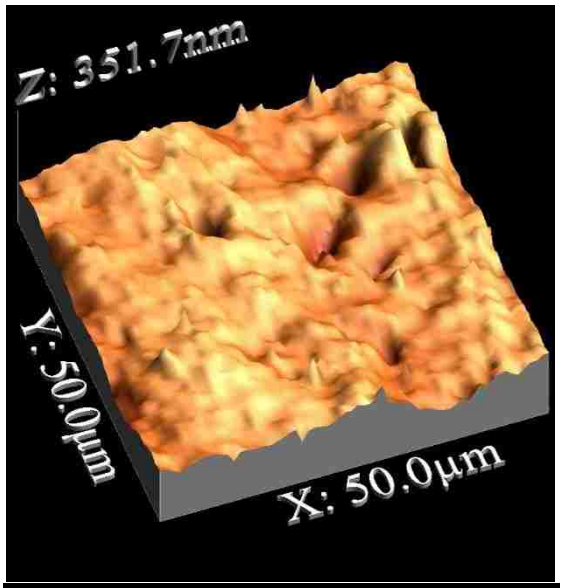

Figure 64 3D image of the surface shown in figure 63.

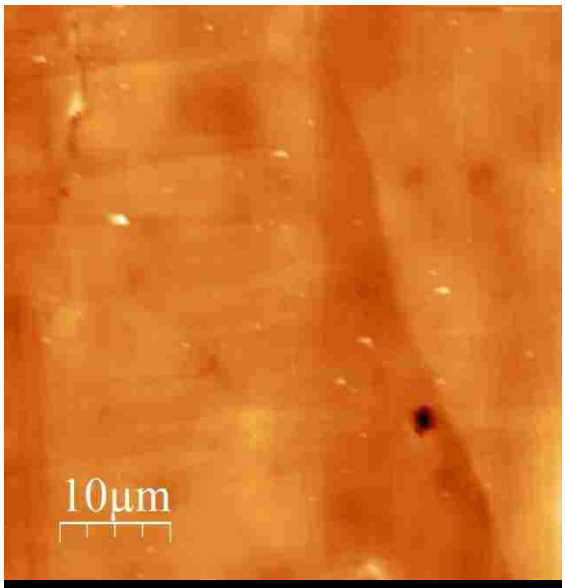

Figure 65 AFM picture of the the area around the middle of the sample about 50 microns to the right of the hole.

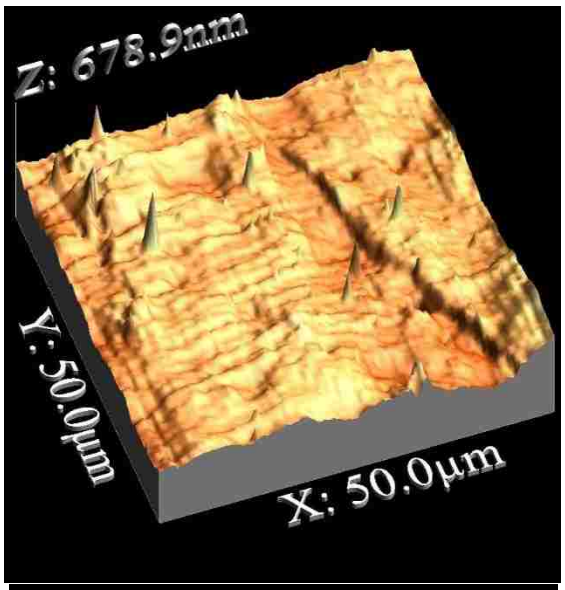

Figure 66 3D image of the surface shown in figure 65.

	RMS roughness	Roughness average
Figure 61,62	28.6713	19.1504
Figure 63,64	25.2903	18.8826
Figure 65,66	39.4323	29.6312

Bottom Right Rough Section

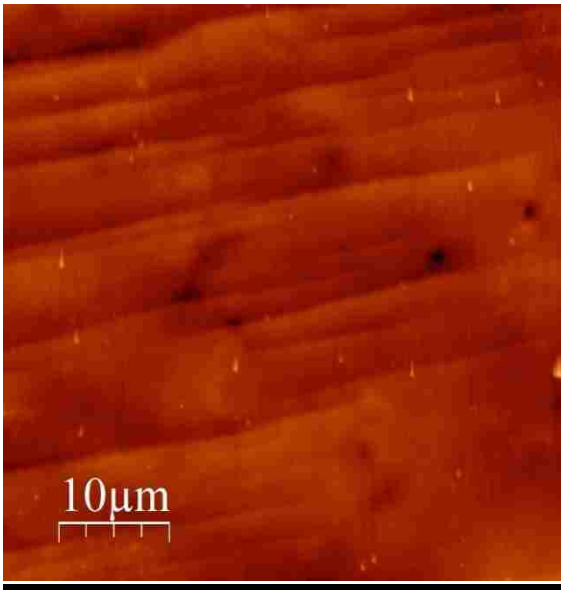

Figure 67 AFM picture of the area starting to show shear banding for the sample about 100 microns away from the hole pulled till yield.

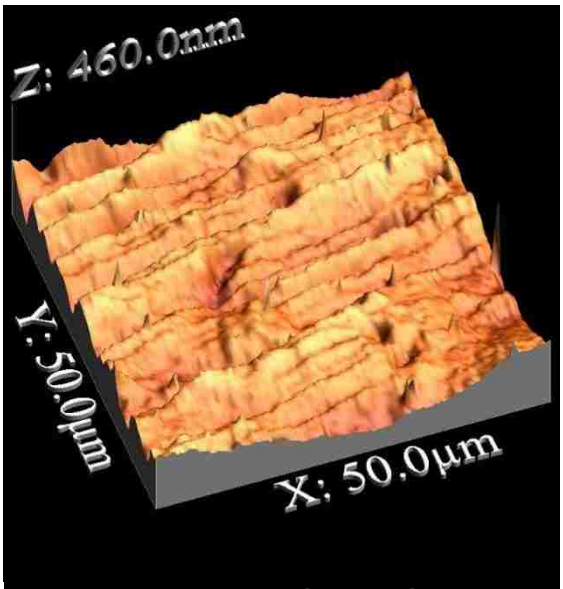

Figure 68 3D image of the surface shown in figure 67.

	RMS roughness	Roughness average
Figure 67,68	32.0771	25.7149

Before Breaking Point Results

Polished

From looking at roughly the same area of the polished section in the sample pulled till just after yield and to the breaking point, we can see that the roughness in the surface are roughly the same. This shows us that all of the stress and strain in the part is being localized to the area around the hole while leaving the rest of the part relatively unaffected.

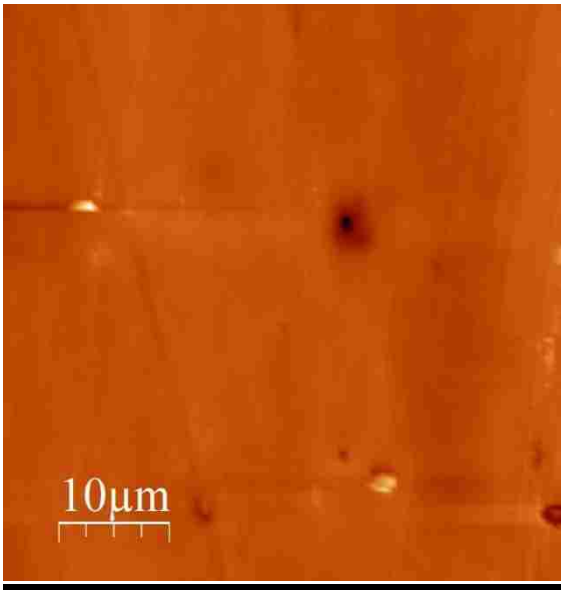

Figure 69 AFM picure of the smooth polished section under the hole for the sample pulled till just before breaking.

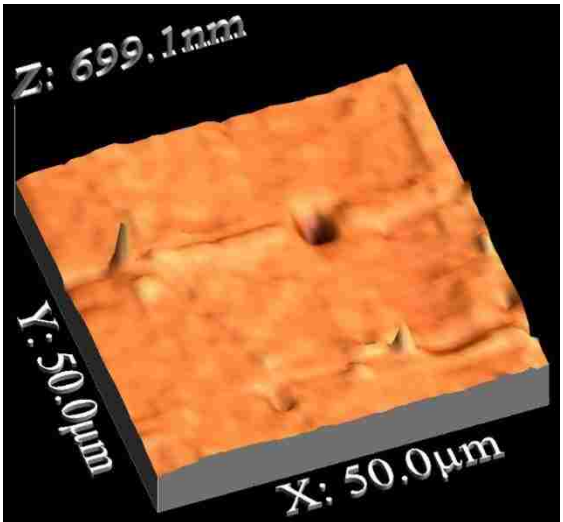

Figure 70 3D image of the surface shown in figure 69.

	RMS roughness	Roughness average
Figure 69,70	21.5122	14.1755

Rough Section

While looking at the roughness in the surface of the part in the bottom right section of the sample pulled to just before break, we can see that surface is about as rough as the yield sample at about 145 nm/μm. This may seem strange because the sample pulled till just before break has deformed a lot more, however because the AFM is not concerned with the angle of the surface and only the roughness this is to be expected. The AFM filter the colors by flattening the colors so that finer details can be observed on the surface rather than the slope of the surface.

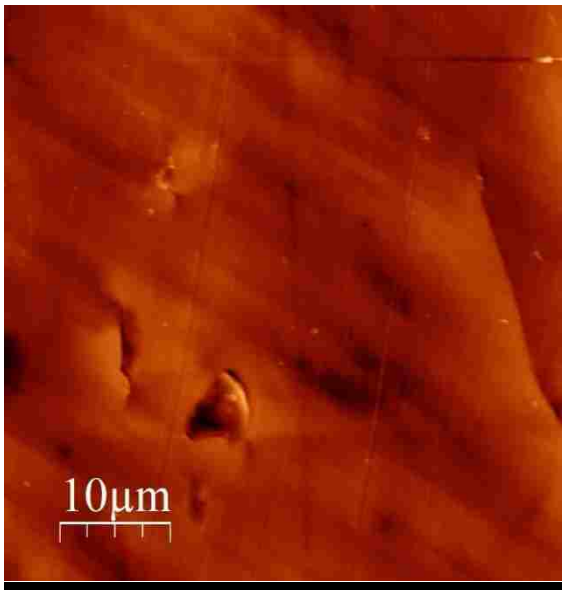

Figure 71 AFM picture the the area about 100 microns below and to the right of hole for the sample pulled till just before breaking.

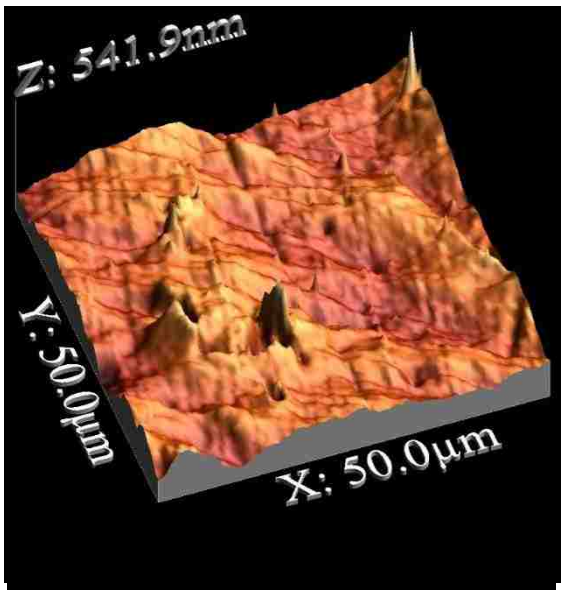

Figure 72 3D image of the surface shown in figure 71.

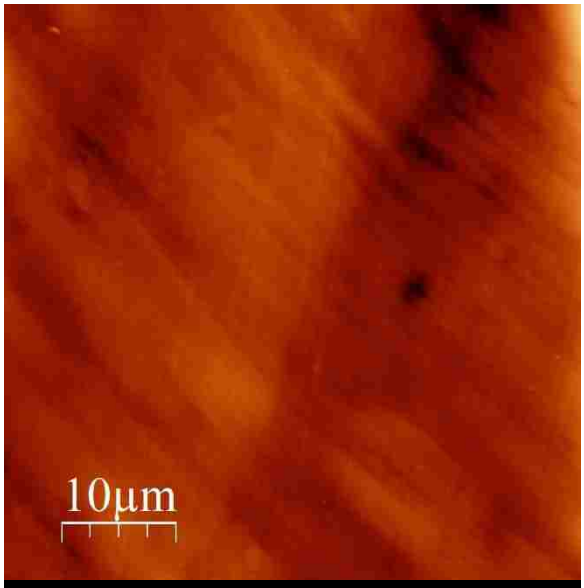

Figure 73 AFM picture the the area about 200 microns below and to the right of hole for the sample pulled till just before breaking.

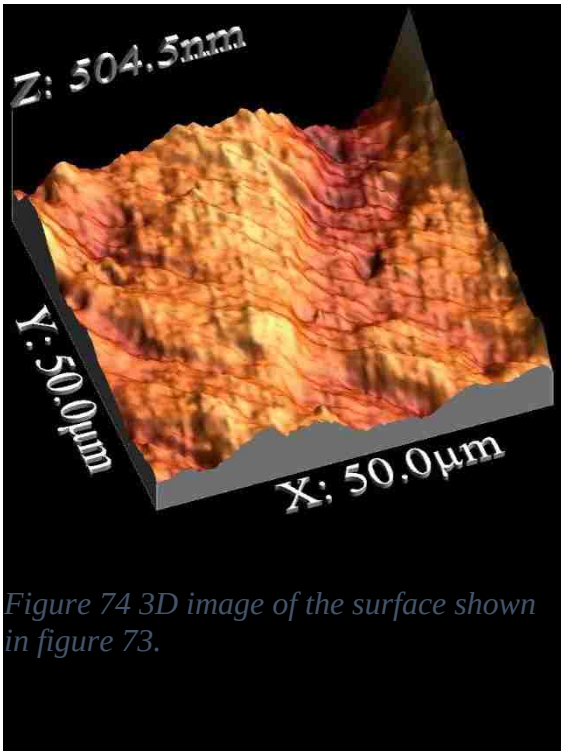

Figure 74 3D image of the surface shown in figure 73.

	RMS roughness	Roughness average
Figure 71, 72	43.6334	34.4417
Figure 73, 74	48.0123	37.4478

Conclusion

After all the various testing and examinations on the different samples, we can conclude that voids and where they are place within the part can influence the structural integrity of the sample. From this we can see that the growth of voids in aluminum follows similar growth patterns of superplastic materials. Placing multiple holes along the cross sectional area in the sample will cause growth to occur soon, while multiple holes in the parallel direction to the tension will delay the increase in the growth size. We can also see from the SEM pictures that the flat shape of the samples removes the questionable results that were gathered from the sample used by Ray that lead to mode III cracking. With the final experiment done to the sample, we saw that the hole in the sample does not only focus the deformation to the area around the hole, which is to be expected, but shows the lack of deformation in certain sections around the hole. These less affected areas seemed to appear directly above, below, left and right of the hole away from the x pattern forming from the shear banding.

Future Work

In future studies there are several factors that could be explored. One question that could be answered is when polishing both sides of the sample would you yield the same results or did the roughness of the opposite side affect the path of the cracks. Another question to be considered is if the size of the hole will affect the void growth of the material. We could also check to see if adding additional holes along the axis of tension might change the void growth rate and how long the part could be stretched before reaching its

breaking point. One last change might be to play around with the way the samples are polished to see if this might also change the visual results.

Appendix A

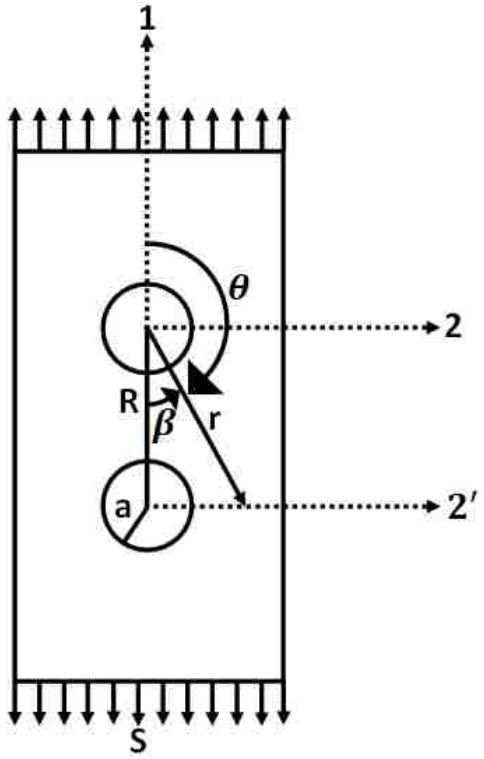

With having the equations for the stress in the different directions an equation for r will need to be created by using R and β.

$$\cos\beta = \frac{R}{r} \qquad \beta = 180 - \theta$$

$$r = \frac{R}{\cos\beta} = \frac{R}{\cos(180-\theta)} \qquad \cos(180-\theta) = \cos 180\cos\theta + \sin 180\sin\theta$$

$$\cos 180 = -1 \quad \sin 180 = 0 \qquad \cos(180-\theta) = -\cos\theta$$

$$r = \frac{-R}{\cos\theta} \qquad r^2 = \frac{R^2}{(\cos\theta)^2} \qquad r^4 = \frac{R^4}{(\cos\theta)^4}$$

Now that we have an equation for r based on θ and R we can now plug this value into our original three stress equations 4-6.

$$\sigma_{rr} = \frac{S}{2}\left(1 - \frac{a^2}{\left(\frac{R^2}{(\cos\theta)^2}\right)}\right) + \frac{S}{2}\left(1 + \frac{3a^4}{\left(\frac{R^4}{(\cos\theta)^4}\right)} - \frac{4a^2}{\left(\frac{R^2}{(\cos\theta)^2}\right)}\right)\cos(2\theta)$$

$$\boldsymbol{\sigma_{rr} = \frac{S}{2}\left(1 - \frac{a^2(\cos\theta)^2}{(R^2)}\right) + \frac{S}{2}\left(1 + \frac{3a^4(\cos\theta)^4}{(R^4)} - \frac{4a^2(\cos\theta)^2}{(R^2)}\right)\cos(2\theta)}$$

$$\sigma_{\theta\theta} = \frac{S}{2}\left(1 + \frac{a^2}{\left(\frac{R^2}{(\cos(\theta))^2}\right)}\right) - \frac{S}{2}\left(1 + \frac{3a^4}{\left(\frac{R^4}{(\cos\theta)^4}\right)}\right)\cos(2\theta)$$

$$\boldsymbol{\sigma_{\theta\theta} = \frac{S}{2}\left(1 + \frac{a^2(\cos\theta)^2}{(R^2)}\right) - \frac{S}{2}\left(1 + \frac{3a^4(\cos\theta)^4}{(R^4)}\right)\cos(2\theta)}$$

$$\sigma_{r\theta} = -\frac{S}{2}\left(1 - \frac{3a^4}{\left(\frac{R^4}{(\cos\theta)^4}\right)} + \frac{2a^2}{\left(\frac{R^2}{(\cos\theta)^2}\right)}\right)\sin(2\theta)$$

$$\boldsymbol{\sigma_{r\theta} = -\frac{S}{2}\left(1 - \frac{3a^4(\cos\theta)^4}{(R^4)} + \frac{2a^2(\cos\theta)^2}{(R^2)}\right)\sin(2\theta)}$$

Now that we have all three of these new stress values we will need to rotate them into the correct direction so that we can add them together to find the proper horizontal stress values.

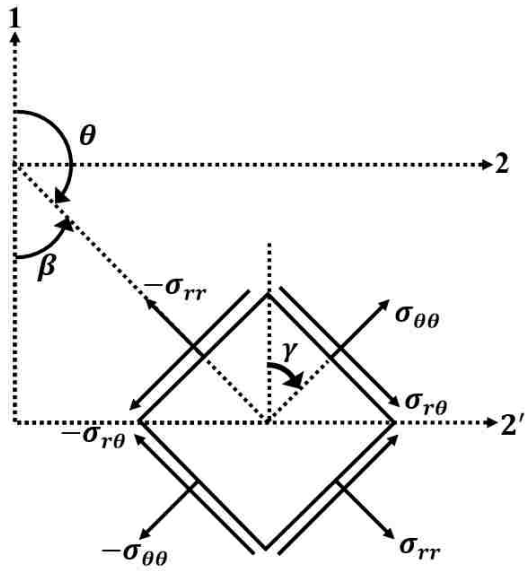

In order to rotate the stress that is being added from the top hole we will need to use the following transformation matrix shown below.

$$\begin{bmatrix} \cos\gamma & \sin\gamma & 0 \\ -\sin\gamma & \cos\gamma & 0 \\ 0 & 0 & 1 \end{bmatrix} = \boldsymbol{\beta} \qquad \begin{bmatrix} \cos\gamma & -\sin\gamma & 0 \\ \sin\gamma & \cos\gamma & 0 \\ 0 & 0 & 1 \end{bmatrix} = \boldsymbol{\beta^T} \qquad \boldsymbol{\beta\beta^T} = \begin{bmatrix} 1 & 0 & 0 \\ 0 & 1 & 0 \\ 0 & 0 & 1 \end{bmatrix}$$

This equation will then be multiplied by the stress matrix in order to get what will be added to the stress values of the bottom hole. When creating the stress matrix we can assume plane stress for the thin plate meaning that all of the stress values in the z direction will be assumed be zero giving us the following matrix.

$$\sigma' = \begin{bmatrix} \sigma_{\theta\theta} & \sigma_{r\theta} & 0 \\ \sigma_{r\theta} & \sigma_{rr} & 0 \\ 0 & 0 & 0 \end{bmatrix} \qquad \sigma = \boldsymbol{\beta^T}\sigma'\boldsymbol{\beta}$$

$$\sigma = \begin{bmatrix} \cos\gamma & -\sin\gamma & 0 \\ \sin\gamma & \cos\gamma & 0 \\ 0 & 0 & 1 \end{bmatrix} \begin{bmatrix} \sigma_{\theta\theta} & \sigma_{r\theta} & 0 \\ \sigma_{r\theta} & \sigma_{rr} & 0 \\ 0 & 0 & 0 \end{bmatrix} \begin{bmatrix} \cos\gamma & \sin\gamma & 0 \\ -\sin\gamma & \cos\gamma & 0 \\ 0 & 0 & 1 \end{bmatrix}$$

σ

$$= \begin{bmatrix} \cos(\gamma) * \sigma_{\theta\theta} - \sin(\gamma) * \sigma_{r\theta} & \cos(\gamma) * \sigma_{r\theta} - \sin(\gamma) * \sigma_{rr} & 0 \\ \sin(\gamma) * \sigma_{\theta\theta} + \cos(\gamma) * \sigma_{r\theta} & \sin(\gamma) * \sigma_{r\theta} + \cos(\gamma) * \sigma_{rr} & 0 \\ 0 & 0 & 0 \end{bmatrix} \begin{bmatrix} \cos\gamma & \sin\gamma & 0 \\ -\sin\gamma & \cos\gamma & 0 \\ 0 & 0 & 1 \end{bmatrix}$$

$$\gamma = 90 - \beta \qquad \beta = 180 - \theta \qquad \gamma = \theta - 90$$

σ

$$= \begin{bmatrix} \cos(\theta - 90) * \sigma_{\theta\theta} - \sin(\theta - 90) * \sigma_{r\theta} & \cos(\theta - 90) * \sigma_{r\theta} - \sin(\theta - 90) * \sigma_{rr} & 0 \\ \sin(\theta - 90) * \sigma_{\theta\theta} + \cos(\theta - 90) * \sigma_{r\theta} & \sin(\theta - 90) * \sigma_{r\theta} + \cos(\theta - 90) * \sigma_{rr} & 0 \\ 0 & 0 & 0 \end{bmatrix} \boldsymbol{\beta}$$

$$\boldsymbol{\sigma_{11}} = (\mathbf{\cos(\theta - 90) * \sigma_{\theta\theta} - \sin(\theta - 90) * \sigma_{r\theta}})\mathbf{\cos(\theta - 90)}$$
$$- (\mathbf{\cos(\theta - 90) * \sigma_{r\theta} - \sin(\theta - 90) * \sigma_{rr}})\mathbf{\sin(\theta - 90)}$$

$$\boldsymbol{\sigma_{12} = \sigma_{21}} = (\mathbf{\cos(\theta - 90) * \sigma_{\theta\theta} - \sin(\theta - 90) * \sigma_{r\theta}})\mathbf{\sin(\theta - 90)}$$
$$+ (\mathbf{\cos(\theta - 90) * \sigma_{r\theta} + \sin(\theta - 90) * \sigma_{rr}})\mathbf{\cos(\theta - 90)}$$

$$\boldsymbol{\sigma_{22} = (\sin(\theta - 90) * \sigma_{\theta\theta} + \cos(\theta - 90) * \sigma_{r\theta}) \sin(\theta - 90)}$$

$$\boldsymbol{+ \ (\sin(\theta - 90) * \sigma_{r\theta} + \cos(\theta - 90) * \sigma_{rr}) \cos(\theta - 90)}$$

Now that we have all three of the stress concentration values that will be added to the stress strictly from a single hole we need to figure out what θ will be needed to add the right stress values.

$$\tan^{-1}\left(\frac{a}{R}\right) \geq \theta \geq \tan^{-1}\left(\frac{0.25}{R}\right)$$

$$R = 0.2088 \ inches \quad a = 0.0632 \ inches$$

$$163.1598813° \geq \theta \geq 129.8686325°$$

References

Ambati, Marreddy, Roland Kruse and Laura De Lorenzis. "A phase-field model for ductile fracture at finite strains and its experimental verification." *Computational Mechanics* (2016): 149-167.

Andrade, FXC, et al. "An Incremental Stress State Dependent Damage Model For Ductile Failure Prediction." *International Journal of Fracture* (2016): 127-150.

Boyce, Brad L, et al. "The Sandia Fracture Challenge: blind round robin predictions of ductile tearing." *International Journal of Fracture* (2014): 5-68.

Briottet, L, JJ Jonas and F Montheillet. "A mechanical interpretation of the activation energy of high temperature deformation in two phase materials." *Acta Materialia* (1996): 1665-1672.

Chen, DC and CS You. "Fracture Criterion for the Tensile Test of 7075 Aluminum Alloy." *Strength of Materials* (2015): 122-127.

Darras, Basil M, et al. "Analysis of damage in 5083 aluminum alloy deformed at different strainrates." *Materials Science and Engineering* (2031): 143-149.

Ghosh, A K and C H Hamilton . "Influences of material parameters and microstructure on superplastic forming." *Metallurgical and Materials Transactions A* (1982): 733-743.

Gurson, Arthur L. "Continuum theory of ductile rupture by void nucleation and growth: Part I - Yeild criteria and flow rules for porous ductile media." *Journal of engineering materials and technology* (1977): 2-15.

Ivanov, Konstantin V and Evgeny V Naydenkin. "Grain boundary sliding in ultrafine grained aluminum under tension at room temperature." *Scripta Materialia* (2012): 511-514.

Jun-Su, Song, et al. "Effect of non-uniform void size and shape distributions on deformation failure in cast aluminum alloy." *Journal of mechanical science and technology* (2012): 2183-2187.

Khaleel, MA, HM Zbib and EA Nyberg. "Constitutive modeling of deformation and damage in superplastic materials." *International Journal of Plasticity* (2001): 277-296.

Khraishi, Tariq A and Yu-Lin Shen. *Introductory continuum mechanics*. 2013.

Khraishi, Tariq A, Mohammad A Khaleel and Hussein M Zbib. "A parametric-experimental study of void growth in superplastic deformation." *International Journal of Plasticity* (2001): 297-315.

Li, Zhenhuan and Minsheng Huang. "Combined effects of void shape and void size--oblate spheroidal microvoid embedded in infinite non-linear solid." *International Journal of Plasticity* (2005): 625-650.

Mae, H, et al. "Comparison of ductile fracture properties of aluminum castings: Sand mold vs. metal mold." *International Journal of Solids and Structures* (2008): 1430-1444.

McClintock, Frank A. "A criterion for ductile fracture by the growth of holes." *ASME* (1968).

Mulholland, Matthew, et al. "Void growth and interaction experiments: Implications to the optimal straining rate in superplastic forming." *International journal of plasticity* (2006): 1728-1744.

Ray, Zachary B. "A Multiscale Study of Plactic Deformation in Voided Materials." University of New Mexico, 2003.

Rice, J R and Dennis Michael Tracey. "On the ductile enlargement of voids in triaxial stress fields." *Journal of the Mechanics and Physics of Solids* (1969): 201-217.

Shikama, Takahiro, et al. "Distinct fatigue crack propagation limit of new precipitation-hardened aluminium alloy." *Scripta Materialia* (2012): 49-52.

Sobczyk, K, J Trebicki and AB Movchan. "Crack path in an elastic material with a random array of small defects." *International journal of fracture* (2004): 103-123.

Tait, R A and DMR Taplin. "Interaction effects during the growth of holes in a superplastically deforming medium." *Scripta Metallurgica* (1979): 77-82.

Takahashi, Yoshimasa, et al. "Fatigue limit investigation of 6061-T6 aluminum alloy in giga-cycle regime." *Materials Science and Engineering* (2014): 243-249.

Tan, Chee Fai and Said Mohd Radzai. "Effect of hardness test on percipitation hardening aluminum alloy 6061-T6." *Chiang Mai Journal of Science* (2009): 276-286.

Tvergaard, Viggo. "Material failure by void growth to coalescence ." *Advanced in applied mechanics* (1989): 83-151.

Wang, YG, ZX Jiang and LL Wang. "Dynamic Tensile Fracture Behaviours of Selected Aluminum Alloys under Various Loading Conditions." *Strain* (2013): 335-347.

Wenjie, Mai. *Fundamental Theory of Atomic Force Microscopy*. n.d. <http://www.nanoscience.gatech.edu/zlwang/research/afm.htm>.

Zeng, Lei, et al. "Fatigue limit of new precipitation-hardened aluminium alloy with distinct fatigue crack propagation limit." *International Journal of Fatiure* (2012): 32-40.

Zhao, Mingjiu, et al. "Hydrogen-induced Modification in the Deformation and Fracture of a Predipitation-hardened Fe-Ni Based Austentic Alloy." *Journal of Material Science & Technology* (2014): 1155-1159.

Zhu, Deju, et al. "Characterization of dynamic tensile testing using aluminum alloy 6061-T6 at intermediate strain rates." *Journal of Engineering Mechanics* (2011): 669-679.